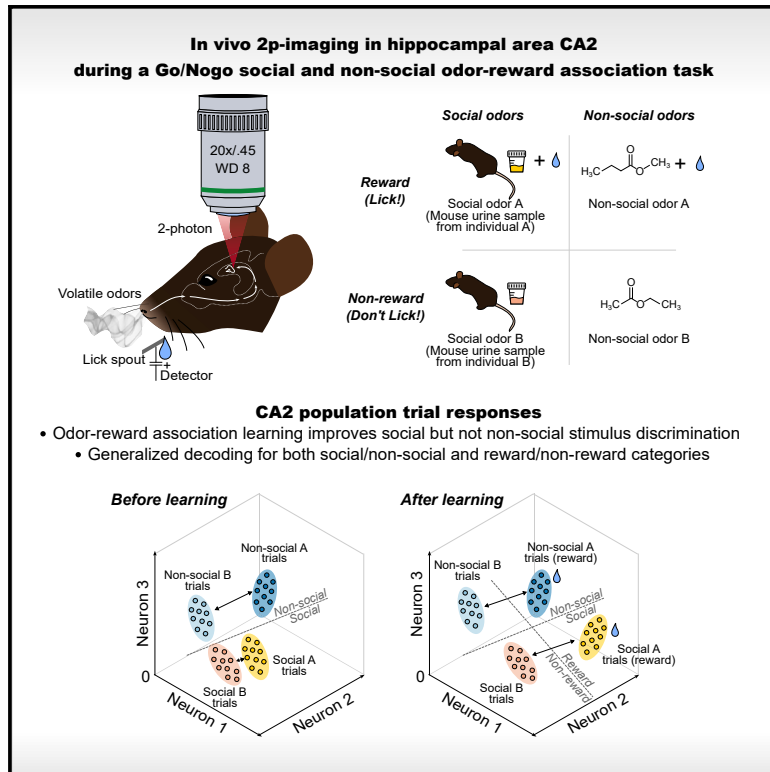


Social odor discrimination and its enhancement by associative learning in the hippocampal CA2 region

Graphical abstract



Authors

Sami I. Hassan, Shivani Bigler,
Steven A. Siegelbaum

Correspondence

sh3432@columbia.edu (S.I.H.),
sas8@columbia.edu (S.A.S.)

In brief

The hippocampal CA2 region is critical for social memory. Hassan et al. report that CA2 responds to and discriminates social odors (urine) from different mice. Social odor-reward learning enhances this discrimination. This suggests that a pre-existing social odor code may incorporate information about rewarding social experiences into social episodic memories.

Highlights

- Hippocampal CA2 pyramidal neuron activity discriminates urine from different mice
- CA2 neurons enable mice to learn to associate a given social odor with a water reward
- Social odor-reward learning enhances CA2 neuron discrimination of social odors
- CA2 responses enable a generalized classification of social versus non-social odors

Article

Social odor discrimination and its enhancement by associative learning in the hippocampal CA2 region

Sami I. Hassan,^{1,2,*} Shivani Bigler,^{1,2} and Steven A. Siegelbaum^{1,3,*}

¹Department of Neuroscience, Mortimer B. Zuckerman Mind Brain Behavior Institute, The Kavli Institute for Brain Science, Vagelos College of Physicians and Surgeons, Columbia University, New York, NY 10027, USA

²These authors contributed equally

³Lead contact

*Correspondence: sh3432@columbia.edu (S.I.H.), sas8@columbia.edu (S.A.S.)

<https://doi.org/10.1016/j.neuron.2023.04.026>

SUMMARY

Although the hippocampus is crucial for social memory, how social sensory information is combined with contextual information to form episodic social memories remains unknown. Here, we investigated the mechanisms for social sensory information processing using two-photon calcium imaging from hippocampal CA2 pyramidal neurons (PNs)—which are crucial for social memory—in awake head-fixed mice exposed to social and non-social odors. We found that CA2 PNs represent social odors of individual conspecifics and that these representations are refined during associative social odor-reward learning to enhance the discrimination of rewarded compared with unrewarded odors. Moreover, the structure of the CA2 PN population activity enables CA2 to generalize along categories of rewarded versus unrewarded and social versus non-social odor stimuli. Finally, we found that CA2 is important for learning social but not non-social odor-reward associations. These properties of CA2 odor representations provide a likely substrate for the encoding of episodic social memory.

INTRODUCTION

The storage and recall of social memory require that neural circuits encode distinct representations of individual conspecifics and their associated experiences. This necessitates the integration of multiple sensory modalities with the outcome and context of social encounters to allow for successful adaptive behavior. Since the early studies of patient H.M.,¹ it has been clear that the storage of social representations requires the hippocampus.² Subsequent studies across a range of species have confirmed the importance of the hippocampus in social cognition.^{3–6} However, our knowledge of how the hippocampus encodes social sensory cues and how those representations may be modified by experience remains poorly understood.

One likely source of sensory information for social memory encoding in rodents is through the olfactory response to social odors. Volatile social odors (urine) are the most salient sensory signal underlying social memory⁷ and other social behaviors⁸ in rodents. Although hippocampal neurons discriminate among non-social chemical odorants,^{9–11} to date, it is unclear whether the hippocampus can detect and/or discriminate between social odors from individual conspecifics and whether those representations can be modified by experience. Because pyramidal neurons (PNs) in the cornu ammonis subregion 2 of the dorsal hippocampus (dCA2) play an important role in the encoding and recall of social memory,^{12–19} we explored social odor responses from these cells using two-photon calcium imaging in awake head-fixed mice.

Previous electrophysiological recordings identified subpopulations of hippocampal PNs that respond to social interactions in freely moving mice, both in dCA2 and in the ventral CA1 region (vCA1), which receives input from dCA2 that is critical for social memory.¹⁴ Such recordings revealed that dCA2 PNs fire in response to social novelty¹⁹ and can distinguish a novel from a familiar animal.^{15,20} In contrast, a fraction of neurons in vCA1 selectively fire in response to a familiar but not novel animal.²¹

However, studies of social representations in freely moving mice are complicated by several factors that impede mechanistic insights. First, the socially relevant information is entwined in the spatial firing properties of both dCA2 and vCA1 neurons.^{15,20–22} Second, studies of social memory in mice rely on the inherent preference of rodents to explore a novel compared with a familiar stimulus. Little is known about whether rodents can form more complex forms of social episodic memory, in which social information is incorporated with a rewarding or aversive social encounter.

Here, we aimed to overcome these limitations by using an experimental paradigm in which we examined the responses of

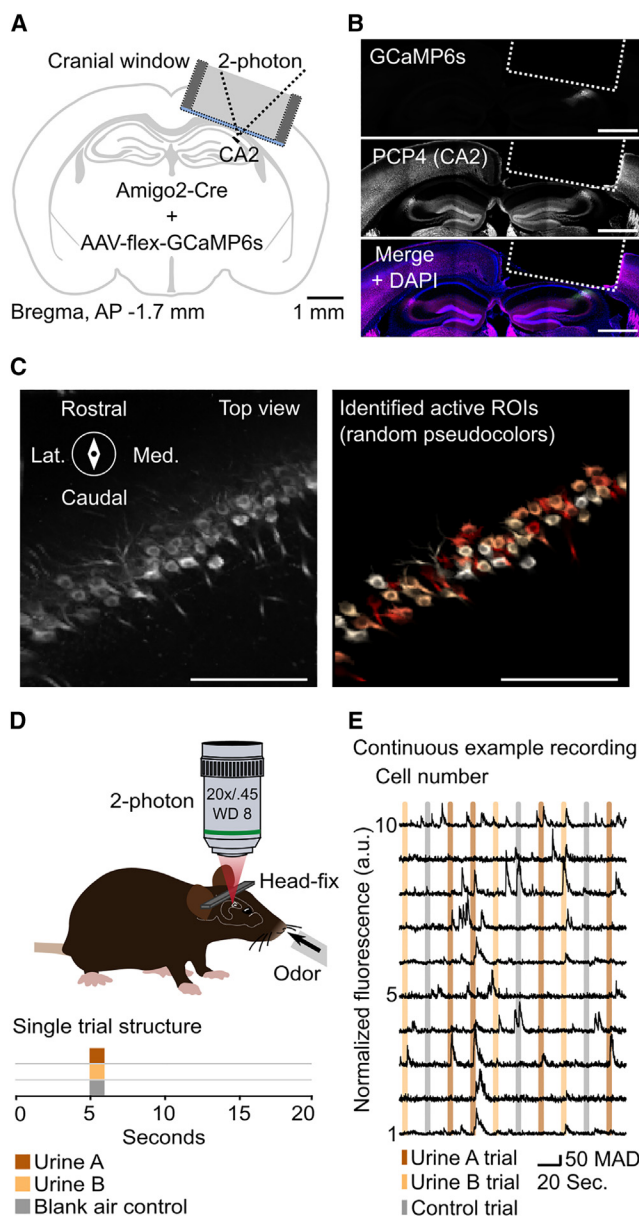


Figure 1. Two-photon calcium imaging of dorsal CA2 PNs during passive social odor presentation

- (A) Two-photon calcium imaging in dCA2 PNs expressing GCaMP6s.
(B) Post hoc confocal images of GCaMP6s expression in dCA2 (top), counterstained with a dCA2 marker (PCP4; middle). Bottom: merged channels. Scale bars: 1 mm.
(C) Left: maximum intensity projection from an example imaging plane. Right: post hoc identified pseudo-colored cell masks (ROIs). Lat, lateral; Med, medial. Scale bars: 100 μm.
(D) Schematic of imaging during social odor presentation to head-fixed, immobilized awake mice. Each odor and blank air control delivered for 1 s in 20 randomized trials.
(E) Continuous normalized fluorescent signals (black traces) with the overlaid timing of color-coded odor/control presentations in ten simultaneously recorded example cells. MAD, median absolute deviation.

dCA2 PNs as a mouse learned to associate a social odor (urine) from one of two male mice with a water reward. We found that the population activity of dCA2 discriminated social odors from novel mice and that this discrimination was enhanced following associative learning. Finally, although populations of dCA2 neurons responded to both social and non-social odors, the geometry of these representations in neural activity space provides a generalizable code that distinguishes social from non-social odors. Thus, like the spatially selective firing of hippocampal place cells, distinct dCA2 representations of “social odor space” emerge rapidly and can be further modified through subsequent experience.

RESULTS

Social odor identity representations in dorsal CA2

We injected Cre-dependent adeno-associated virus (AAV) in the dCA2 region of Amigo2-Cre mice¹² to selectively express GCaMP6s²³ in dCA2 PNs (Figures 1A–1C). We then used a two-photon microscope to image through a cranial window²⁴ the calcium responses of dCA2 PNs as a head-fixed mouse was exposed to different social odors (urine from age-matched C57Bl/6J males; Table S1) or a blank air control (Figure 1D). Post hoc colabeling with a dCA2 PN marker confirmed the specificity of GCaMP6s expression. *In vivo*, dCA2 PN soma appeared as a diagonal band across the imaging plane (Figure 1C), with 115 ± 21 (mean \pm SD) PNs becoming active per recording session. A single trial consisted of a 1-s-long presentation of either an odor or blank air control. Trials were repeated once every 20 s, and each stimulus was delivered 20 times, resulting in a total of 60 randomly ordered trials (Figure 1E).

To identify potential stimulus-evoked activity in dCA2, we sorted trials by their respective stimulus type and plotted the median trial activity of individual cells as a function of time. This revealed subsets of cells whose activity increased or decreased, relative to baseline, in response to one or more urine samples; very few cells responded to blank air presentations (Figure 2A). Single-trial analysis further confirmed robust odor-evoked responses in a fraction of cells. Some cells responded to both urines whereas others responded selectively to a single urine (Figure 2B).

The specificity of odor responses was evaluated with a receiver-operating characteristic (ROC) analysis^{25,26} (Figure 2C). For each neuron, we compared the trial activity distribution before (baseline) and after stimulus presentation (Figure S1A). A neuron was identified as odor-activated when the area under the ROC curve (AUC) and the derived selectivity index was greater than 97.5% of values from a shuffled distribution and odor-inhibited when the AUC was less than 97.5% of shuffled values (Figure S1B). Overall, ~25% of the total population of dCA2 neurons was either activated or inhibited in response to either urine (Figure S2A). We found 10% of dCA2 neurons were significantly activated with urine A and 9% with urine B, greater than the 2.5% chance level. Most of the odor-activated neurons responded to both urines, amounting to 6% of the total dCA2 population; 4% of PNs were selectively activated by urine A and 3% by urine B. A slightly larger fraction of dCA2 cells was inhibited with urine A (14%) and urine B (15%), with 6% of neurons

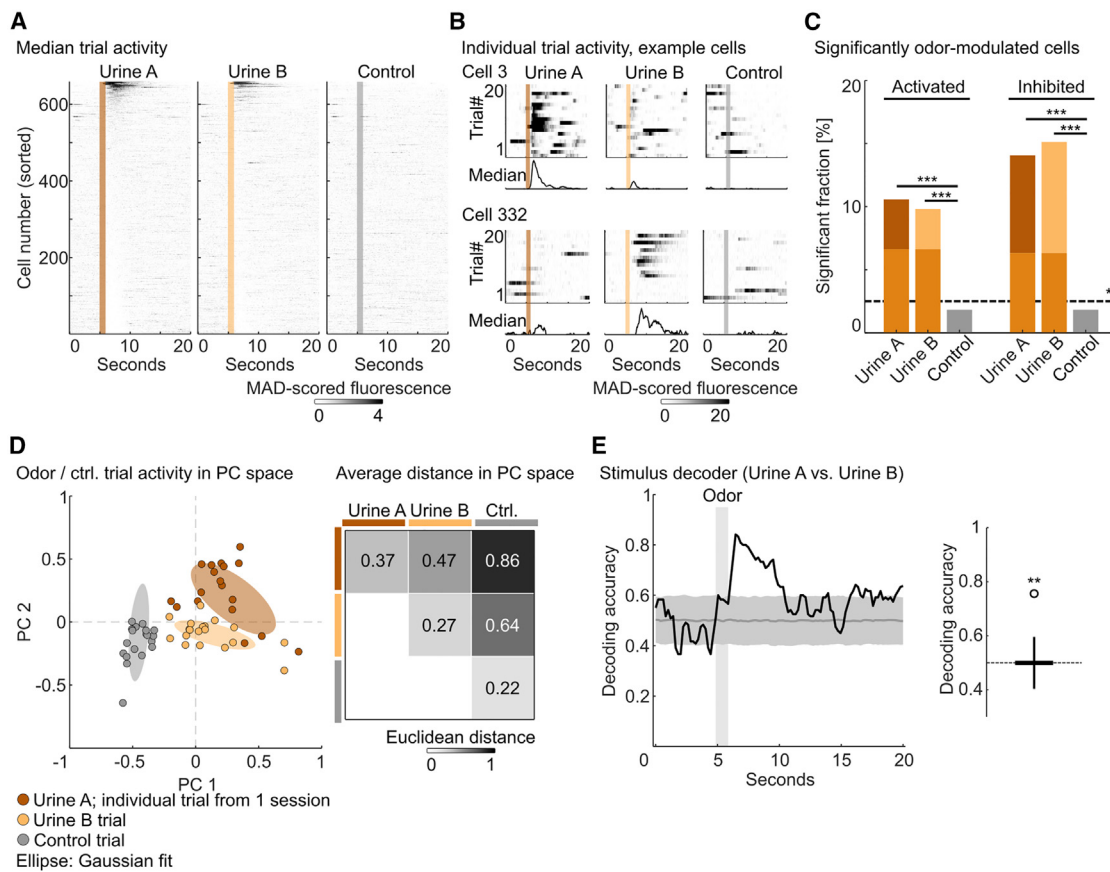


Figure 2. Stimulus tuning and decoding accuracy in dorsal CA2

(A) Median trial activity in response to indicated stimuli as a function of time (659 cells, seven animals; same for C–E). Cells are sorted by ascending average odor response measured zero to 3 s after odor onset during presentation of urine A. Cell sorting is constant across conditions.

(B) Single trial responses (raster plots) and the median activity (trace at bottom) across trials of two example cells. Trials are arranged by the stimulus condition.

(C) Stimulus tuning in dCA2. ROC analysis-based distribution of fraction of cells significantly activated (left bars) or inhibited (right bars) relative to baseline by indicated stimulus presentation. The fraction of cells activated specifically by one odor is shown at the top part of the bar; the bottom part shows the fraction of cells activated by both odors. *, 95% confidence (dashed line) based on a two-sided permutation test (see also Figure S1C). The fraction of cells activated or inhibited by each odor was significantly greater than the fraction of cells responding to blank air control trials: ***, p < 0.001; two-sided Fisher's exact test.

(D) Left: first two principal components of dCA2 population trial responses, averaged over a 3-s window after stimulus presentation to social odors or blank air control. Individual points represent projections of averaged activity during a single trial for each of the 20 trials in a given condition. Separate two-dimensional Gaussian models are fit to each stimulus trial data (ellipses; mean \pm 1 SD). Units: normalized fluorescence. Right: average Euclidean distance in the principal component space within and across trial clusters.

(E) Left: population-decoding accuracy of stimulus identity (binary linear SVM, control trials excluded) as a function of time. Black line: cross-validated mean; shading: chance decoding from shuffled distributions (mean \pm SD). Right: significance was determined based on the difference between average decoding accuracy (0.76, circle) and chance (bar: 0.5 ± 0.1 , mean \pm 1 SD), measured zero to 3 s after odor presentation. **, p < 0.01; Z score significance test.

inhibited by both urines and 8% and 9% of PNs inhibited selectively by urine A and B, respectively. In contrast, only 2% of dCA2 cells were significantly activated and 2% significantly inhibited by blank air delivery, equal to chance levels (Figures 2C and S1C). The frequency of odor-activated and/or odor-inhibited cells was significantly larger than chance levels and greater than the fraction of cells that were activated or inhibited in response to blank air (Figures 2C and S2A).

To examine whether the dCA2 PN population discriminated among social odors and blank air controls, we performed a principal-component analysis (PCA) on activity vectors of the pseudo-population of 659 cells recorded from seven mice. For

each cell in each trial, we averaged the calcium responses in a 3-s-long window following odor presentation. The first two principal components captured 18% of the variance and revealed distinct clusters in principal component space for the two urine and blank control trials. Blank air and urine responses were separated along the axis of the first principal component, whereas the responses to the two urine samples were separated along the axis of the second component (Figure 2D).

Next, we used a binary linear decoder to examine the information encoded in the full dimensions of the dCA2 pseudo-population neural activity space. We averaged the neural responses for each 20-s-long trial in 200-ms-long bins and trained a binary

linear support vector machine (SVM)²⁷ to distinguish responses to the two urine samples for each time bin, using 80% of trial data. Decoding performance was tested on the 20% remaining held-out trials (Figure 2E). Chance levels of decoding were obtained by the decoding performance from 1,000 random shuffles of trial labels (mean \pm SD). Before odor onset, the classifiers performed at chance. Once the odor reached the nose port (~ 1 s after the odor valve opened), decoding accuracy sharply rose to reach a level significantly above chance and then decayed back to chance levels during the inter-trial interval. Decoding based on data from individual animals, instead of the pseudo-population, confirmed the significant social odor identity decoding in the dCA2 population (Figure S2B).

The accuracy of odor identity decoding in dCA2 can result from either the highly odor-selective responses of a subpopulation of cells or a population-based response of cells with weak, mixed selectivity.²⁸ To distinguish between these possibilities, we repeated the decoding analysis excluding the significantly odor-activated cells identified by ROC analysis. Decoding with the residual population failed to rise above the chance level (Figure S2C, second bar plot). In contrast, decoding accuracy using only the 13% of cells that were significantly activated by one or both odors was comparable with results from the whole population (Figure S2C, third bar plot). Thus, decoding accuracy was driven by the subset of cells significantly activated by odor. In contrast, the performance of a decoder trained only with the 23% of cells that were significantly inhibited by an odor failed to rise above chance levels (Figure S2C, fourth bar plot).

Associative learning enhances social odor tuning in dorsal CA2

Given the distinct representations of novel social odors in dCA2, we next examined how these representations might be affected by the association of an odor with an extrinsic experience—the delivery of reward. We presented the same two social odors to water-deprived mice in a Go/No-Go associative reward learning task¹⁰ in which urine A was paired with a water reward, whereas urine B and control trials were unrewarded (Figures 3A and 3B). Mice rapidly learned to lick in response to odor A and to withhold licking to either odor B or blank air, reaching a criterion of 80% correct trials after 2–5 days of training (Figures 3C and 3D). A logistic fit that modeled group learning crossed the criterion level on day 4 and reached a maximal accuracy of 100% (Figure 3D, bottom left). As discussed below, we imaged dCA2 activity to odor presentation before training (phase I; as described in Figures 1 and 2 above), during training, and for 2 days after reaching the criterion (phase II).

As social behavior often requires flexible adaptation, we also examined mouse behavior and dCA2 odor coding on switching reward contingency, rewarding odor B instead of A (Figures 3C and 3D). We recorded mouse behavior and dCA2 activity immediately after switching the contingency (phase III) until mice had learned the new reward contingency (phase IV). Reversal learning proved challenging, with only five of the eight mice reaching the criterion following the contingency switch. A fit of the logistic model to all eight mice reached a maximal accuracy of only 70%, less than the 80% learning criterion (Figure 3D, bottom right).

To explore whether initial or reversal reward learning altered dCA2 social odor representations, we pooled cells from all recorded animals with stable recordings during the initial reward learning (six of the eight mice for phases I and II) and during reversal learning (using three of the six mice with stable implants in phases III and IV, those reaching the criterion; see Figure 3D for details). An ROC analysis of the initial reward learning (phase I versus phase II) revealed a significant increase in the fraction of cells that were selectively activated by the rewarded odor but not by the unrewarded odor (Figure 3E, left). The effect of learning was even more pronounced for the inhibited neurons (Figure 3E, right), with significant increases in the fraction of neurons selectively inhibited by the rewarded odor after both the initial reward learning (phase I versus phase II) and following reversal learning (phase III versus phase IV).

Dorsal CA2 population activity forms flexible social odor-reward associations, improving decoding of stimulus identity

We next explored the effect of learning on odor coding at the dCA2 PN population level. PCA was performed on the pseudo-population of cells that were reliably identified across different phases of learning²⁹ (Figures S3A–S3D). The projected values for the first two principal components during responses to the two odors overlapped in the first session of reward-association learning (Figure 4A), when the mice performed at chance levels (phase I). However, there was a clear separation between the control and odors responses (Figure 4A, top row), which we quantified using the Euclidean distances between the response clusters (Figure 4A, bottom row); whereas the distance between the two odor clusters was similar to their within-cluster distances (a measure of a cluster's trial variance), the distance between a given odor cluster and the control cluster was significantly greater than the within-cluster distance.

Odor-reward learning produced a striking alteration in the dCA2 PN odor responses, leading to a clear separation in the odor response clusters in the principal component space after mice reached the criterion (phase II). The trial clusters for odor A, odor B, and blank air control were now all separated (along principal axis one), with the rewarded social odor cluster (urine A trials) having the largest distance from the control trials. After switching the reward contingency, which caused an initial drop in performance back to the chance level, the distances among the three trial activity clusters in the principal component space collapsed, resulting in the overlap of all three response clusters. Strikingly, on learning the new reward contingency (phase IV), the response clusters separated, with the newly rewarded social odor B becoming the most distinct cluster. Of interest, following reversal learning, the three response clusters separated along a principal component axis (component two) orthogonal to the axis that separated the responses after the initial reward learning (phase II), indicating that the two reward associations recruited independent activity patterns.

Both single-cell analysis and PCA suggested that dCA2 incorporates valence into stimulus representations, thereby enhancing odor stimulus discrimination. To further test this idea, we asked whether learning affected the accuracy of odor response decoding by a linear classifier. Indeed, although the

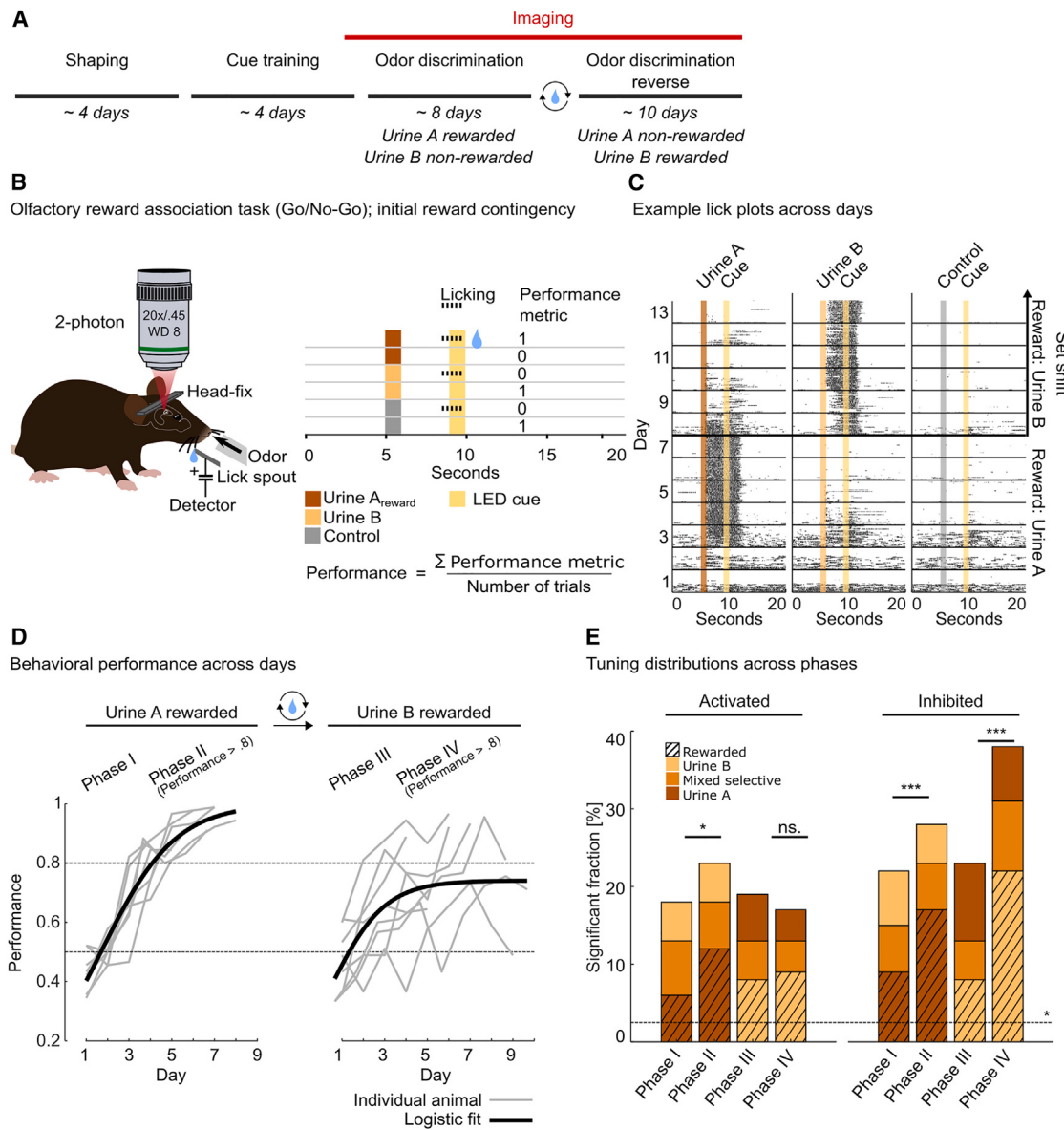


Figure 3. Adaptive social odor-reward association learning in mice using a Go/No-Go operant conditioning task

(A) Timeline of recording dCA2 activity during the social odor-reward learning task.

(B) Schematic of the behavioral setup, the task structure, and the outcome metric to calculate a performance index. Mice were presented with urine A, urine B, or blank air control odors. Only urine A was paired with a water reward, delivered at the end of a 1 s LED cue if an animal licked during the cue period. See text for further details.

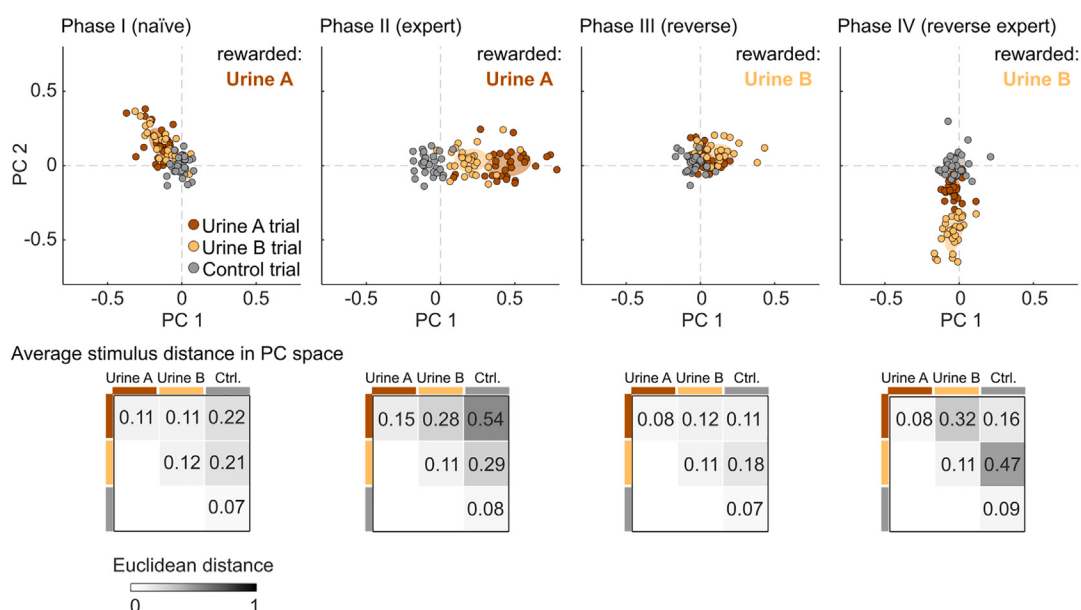
(C) Example lick plot from an individual animal performing the task across 13 days. Each day consisted of 90 random trials (30 presentations of each odor or blank air). Lick responses to odors are shown for individual trials during each day, sorted in columns according to odor, with early trials at the bottom and late trials at the top for each day. Days are stacked on top of one another. Black tick marks, individual lick contacts with the spout; colored/gray bars, stimulus presentation; yellow bars, cue window; horizontal gray lines separate individual days; thick black horizontal line, set shift in reward contingency.

(D) Behavioral performance across days. The learning trajectory was classified into four phases: phase I, the first day of training (urine A rewarded); phase II, sessions after a mouse reached criterion of >80% correct trials; phase III, the 1st day of reward reversal (urine B rewarded); and phase IV, sessions after mice reached criterion after contingency reversal. Lower panels, learning curves for individual animals (light gray lines), before (left), and after (right) reward reversal. Learning data fitted by a three-parameter logistic model (black lines): left, maximal performance = 1, slope = 0.006 [1/trials], midpoint = 152 [trials]; 8/8 mice reached criterion. Right, maximal performance = 0.7; slope = 0.009; midpoint = 36; 5/8 animals reached criterion.

(E) Stimulus tuning during reward learning. ROC distributions of significantly activated or inhibited dCA2 PNs (relative to baseline) during indicated phases. Bars, fraction of cells responsive selectively to urine A (dark shade), non-selectively to urine A and B (medium shade), or selectively to urine B (light shade): left, activated cells. Right, inhibited cells. Hash marks indicate rewarded odor. *, 95% confidence (dashed line); two-sided permutation test. ***, p < 0.001; *, p < 0.05; ns., p > 0.05; two-sided Fisher's exact test. phase I-III, n = 6 animals (two mice excluded due to unstable recordings); and phase IV, n = 3 animals (only three of six mice with stable window implants reached the criterion).

A

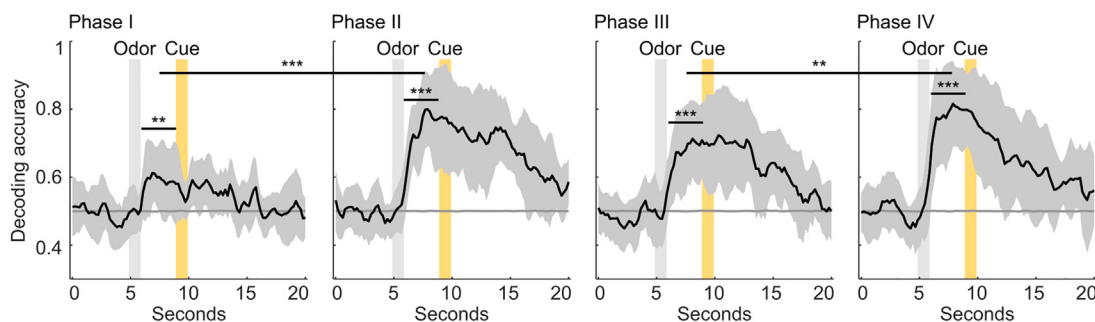
Trial averages projected in common PC space across different learning phases



B

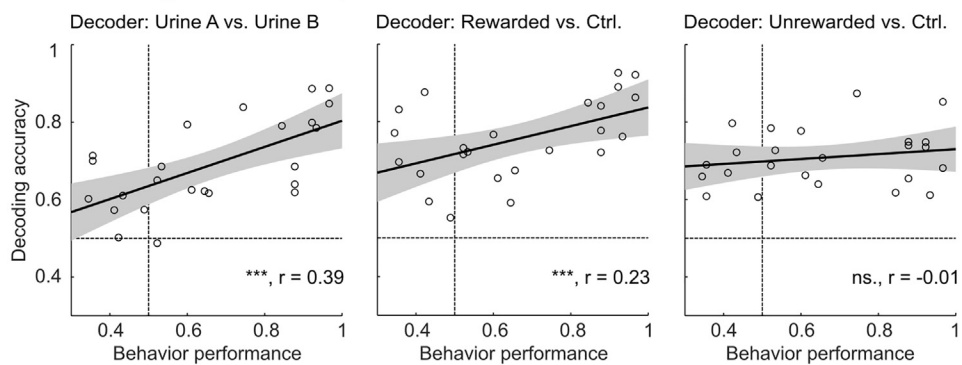
Stimulus decoding accuracy across phases

Stimulus decoder
Urine A vs. Urine B



C

Behavior-decoding correlation across phases



(legend on next page)

classifier decoded urine A from B at an accuracy greater than chance in all four phases of the task, decoding accuracy significantly increased after learning, both with the initial learning and with reversal learning (Figure 4B). Interestingly, we could decode rewarded urine A from non-rewarded urine B after learning using either the subset of odor-activated cells or the subset of odor-inhibited cells, whereas the odor-inhibited cells failed to decode urine A from urine B prior to learning (Figure S4; see also Figure S2B, fourth bar).

To examine whether the increased decoding accuracy was related to behavioral performance, we plotted decoding accuracy versus behavioral performance for all animals (including animals that did not reach the criterion after the contingency switch) during all sessions. We observed a highly significant correlation, based on the Pearson correlation coefficient, between odor decoding accuracy and behavioral performance (Figure 4C, left). We also found a significant correlation between the accuracy of decoding a rewarded social odor (either A or B) from blank air control with behavior (Figure 4C, middle). However, there was no significant correlation between the decoding of the non-rewarded odor (either A or B) from blank air control with behavior (Figure 4C, right).

Stability of stimulus decoding in dorsal CA2

As the odor-reward association behavior reached a high level of performance that persisted over several days, we next assessed the stability of odor representations following learning. We trained a decoder to distinguish urine A from B on the first day an animal reached the learning criterion (day n) and then tested the decoder on the activity of the same cells in the subsequent session (day n + 1). We found significant decoding across a single day, both immediately after the mice reached the criterion (n versus n + 1) as well as from the second to the third day of expert performance (n + 1 versus n + 2; Figure S5A). Significant decoding was also observed when training and testing sessions were 2 days apart in phase II (day n versus n + 2) (Figure S5B, left). Interestingly, significant stimulus identity decoding was still possible when we trained a decoder 2 days before the contingency switch and tested it on the session immediately after switching the reward contingency (day n versus n + 2), although the decoder performance was less than when reward contingency was constant between training and testing sessions (Figure S5B, right). Therefore, dCA2 provides consistent stimulus identity information to a downstream readout, at least over the course of 2 days.

Figure 4. Social odor discrimination is enhanced following social odor-reward learning

(A) Top row: first two principal components of dCA2 population trial responses for indicated learning phases. Individual dots, projections of single trials. A two-dimensional Gaussian model is fit to each stimulus trial data (ellipses; mean \pm 1 SD). Units: normalized fluorescence. Lower row: average within and across trial-cluster distances (Euclidean) in the PC space. Compared with the passive odor presentation results of Figure 2, odor clusters show greater overlap in phase I. This may reflect the unexpected presence of the unlearned water reward in phase I and/or the lower number of cells due to the longitudinal tracking ($n = 447$ versus $n = 659$ in Figure 2). $n = 6$ animals in phase I–III; $n = 3$ animals in phase IV (same for B).

(B) Decoding accuracy of stimulus identity (binary linear SVM decoder, control trials excluded) as a function of trial time in individual animals. Independent decoders were trained for each session. Significance was determined by the difference between average decoding accuracy (phase I: 0.59 ± 0.08 ; phase II: 0.73 ± 0.09 ; phase III: 0.67 ± 0.08 ; phase IV: 0.77 ± 0.10) and chance (0.50 in all four phases), averaged 0–3 s after odor presentation. Shading: mean \pm 1 SD; average chance decoding is shown by the gray line. **, $p < 0.01$; ***, $p < 0.001$; one-sided paired bootstrap significance test.

(C) Behavior-decoding correlation. Decoders trained to distinguish between urine samples (left), rewarded odor (urine A before and urine B after set shift) versus blank air control (middle), and unrewarded odor versus blank air control (right). Decoding performance from individual sessions with six animals across the four phases plotted as open circles. A linear regression line (thick black line) and its 95% confidence interval (shading) are overlaid, chance levels (0.5) are indicated by the dashed lines; ***, $p < 0.001$; ns, $p > 0.05$.

Dorsal CA2 pyramidal cells primarily respond to stimulus identity and behavioral choice

Might the enhanced odor discrimination by dCA2 following learning reflect the behavioral choice associated with the odor or a motor response to licking, rather than odor-reward memory? To address these questions, we first compared dCA2 responses during correct and incorrect trials in a given session, focusing on the learning phase before the criterion to obtain a sufficient number of error trials. We further restricted our analysis to trials with unrewarded odor B, whose higher behavioral error rate than odor A trials provided sufficient statistical power (Figure S6A).³⁰ For each cell, we determined its ROC-based selectivity index (see Figure S1A) separately for correct and error trials. A plot of the selectivity indexes in error trials versus correct trials revealed a significant positive correlation, arguing that the neural response selectivity was determined to a significant extent by stimulus identity rather than by the behavioral choice alone (Figure S6B).

In addition to the significant overall correlation in tuning between correct and error trials, many cells showed differential responses. We therefore used population decoding to test whether a decoder could classify correct (licking to odor A or withholding to odor B) from incorrect (licking to odor B or withholding to odor A) trials. The classifier decoded the choice above chance, time-locked to the odor presentation (Figure S6C, left and right). Choice-based decoding accuracy, however, was significantly lower than decoding based on the stimulus identity (Figure S6C, middle and right).

To further exclude the possibility that decoding was solely based on choice or motor signals, we repeated the decoding analysis using those urine A/B trials where the animals licked to each odor (same choice and motor behavior, different stimuli). This decoder performed with similarly high accuracy as a decoder trained on both lick and no-lick trials (Figure S6C, right, second and third bar plots). Furthermore, a decoder failed to distinguish lick versus no-lick trials when trained on blank air trials only (Figures 6D and 6E), further indicating that dCA2 activity did not reflect lick-related or motor signals.

Dorsal CA2 activity decodes social odor identity irrespective of reward association

To further assess the nature of enhanced social odor decoding after reward learning, we trained animals with a set of four novel social odors (urine C–F; Figure 5A), two of which were rewarded (urine C and E) and two of which were not (urine D and F). All

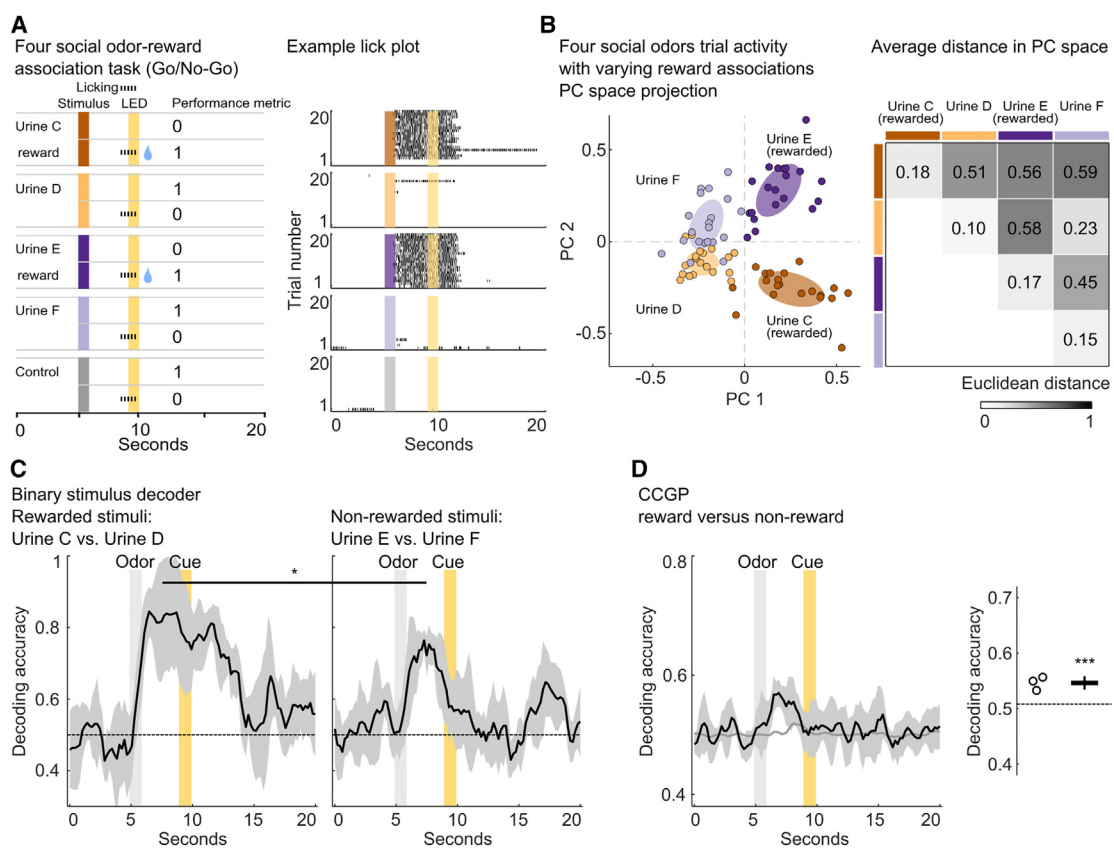


Figure 5. Dorsal CA2 activity discriminates social odor identity and provides a generalized reward classification

(A) Left: schematic of social odor-reward learning task with two rewarded and two unrewarded social odors and metric used to calculate performance. Right: lick behavior of a well-trained animal performing above criterion (>80% correct responses).

(B) Left: first two principal components of dCA2 population trial responses after learning. Individual dots represent projections of single trials. A two-dimensional Gaussian model is fit to each stimulus trial data (ellipses; mean ± 1 SD). Units: normalized fluorescence. Right: average Euclidean distance in PC space within and across trial clusters. n = 3 animals.

(C) Decoding accuracy of stimulus identity (binary linear SVM, control trials excluded) as a function of time for individual animals. Decoding of stimuli was run separately within reward category (rewarded odors, left; non-rewarded odors, right). Average decoding accuracy for rewarded (0.82 ± 0.1) and non-rewarded odors (0.71 ± 0.07) differed significantly; *, p < 0.05; one-sided paired bootstrap significant test; n = 3 animals (same in D). Shading: mean ± 1 SD; average chance decoding shown by the dashed line.

(D) Cross condition generalization performance (CCGP). Left: a linear binary decoder (SVM) was trained on one rewarded/non-rewarded odor pair (e.g., urine C versus urine D) and tested on the remaining odor pair (urine E versus urine F; see also Figure S7B). Shading: mean ± 1 SD. Right: circles, individual animal CCGP values; bars, mean ± 1 SD CCGP = 0.55 ± 0.01 . ***, p < 0.001 relative to chance (0.5); one-sided paired bootstrap significance test.

animals readily learned this task and reached the criterion (e.g., Figure 5A, right). After learning, the four odors showed distinct activity clusters in the principal component space, separated into odor identity and reward classes (Figure 5B). The first two principal components captured 15% of the variance, with principal component one separating rewarded from non-rewarded odors. The total within-cluster Euclidean distance to a given odor was small (diagonal values) compared with the across-cluster distances. Unrewarded odors clustered closer together than rewarded odors, again suggesting that reward association or reward expectancy might enhance discrimination. However, odors within a given category (rewarded or non-rewarded) were also clearly separable and a Euclidean distance classifier trained on the full vector space accurately decoded all odor and control trials based on stimulus identity (Figure S7A). This

suggests that dCA2 encodes both odor identity and reward valence.

We then trained two binary linear classifiers to distinguish odors within their respective reward category. Both the rewarded odor classifier as well as the non-rewarded classifier performed with high accuracy after the odor onset; however, decoding accuracy in the non-rewarded case was significantly lower than that in the rewarded case (Figure 5C). These complementary and independent sets of results clearly show that the dCA2 neural population can discriminate social odor identity based on the sensory properties of the odors in a manner that was refined by, but not solely dependent on, reward association, a prerequisite of social discrimination and social value associations.

To determine whether dCA2 may provide a general classification of reward category independent of stimulus identity,

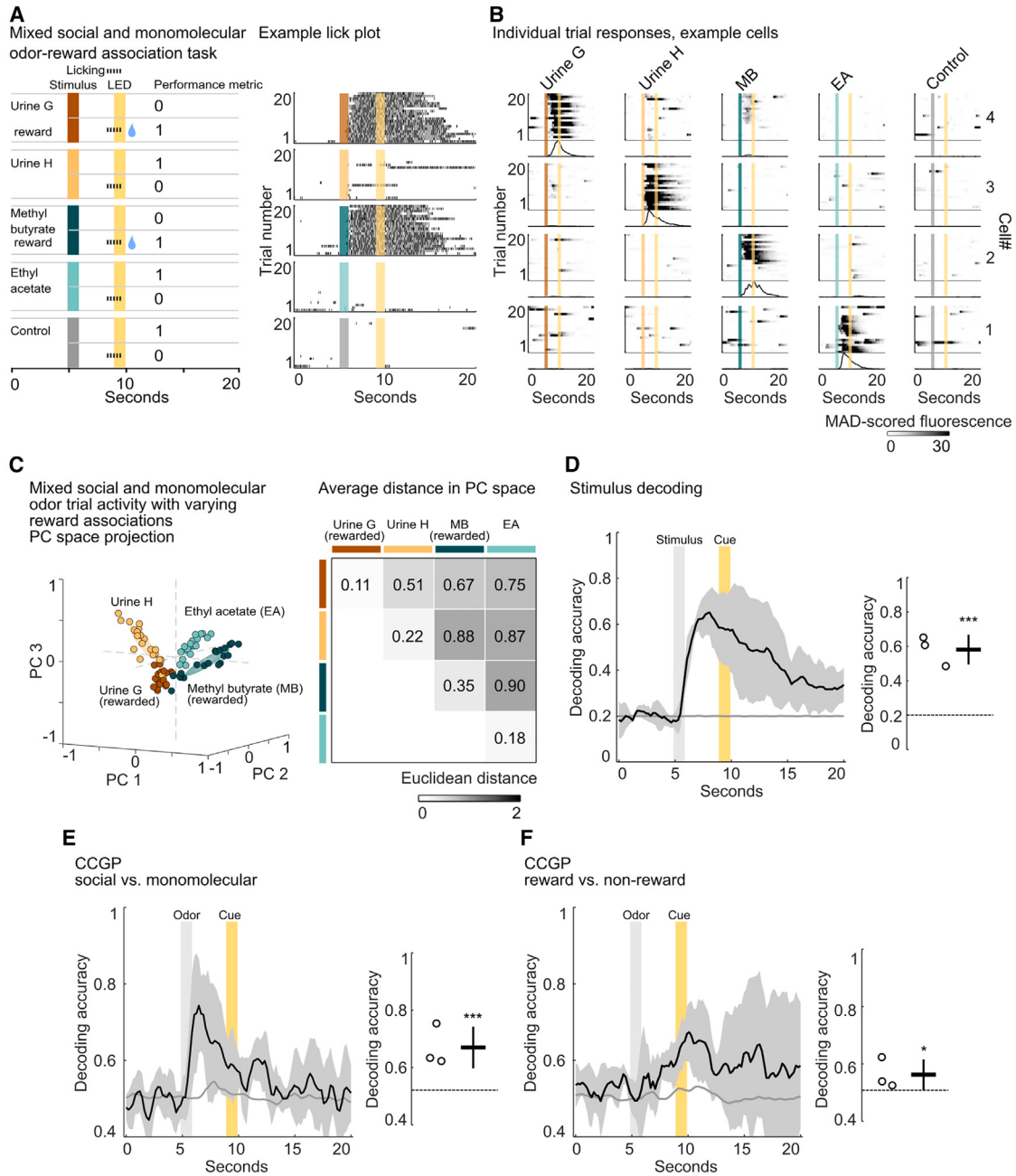


Figure 6. Dorsal CA2 encodes generalized representations of social versus non-social odors

(A) Left: schematic of odor-reward association task using two social and two non-social odors, one of each being rewarded, and outcome metric. Right: lick plot of an animal performing above criterion (>80% correct).

(B) Single-trial responses (raster plots) of four example cells, each tuned specifically to one of the four odors and their median activity across trials. MB, methyl butyrate; EA, ethyl acetate.

(C) Left: first two principal components of dCA2 population trial responses to two social odors and two monomolecular odors. A two-dimensional Gaussian model is fit to each stimulus trial data (ellipses; mean \pm 1 SD). Units: normalized fluorescence. Left: average within and across trial-cluster Euclidean distance in PC space. n = 3 animals.

(legend continued on next page)

we determined the cross-condition-generalized-performance (CCGP) decoding accuracy, as defined by Bernardi and colleagues.³¹ CCGP was measured by training a reward decoder on one rewarded/non-rewarded odor pair and testing the trained model on data from the odor pair that was excluded from training (Figure S7B). Indeed, CCGP was significantly greater than chance and time-locked with the odor presentation (Figure 5D). This generalized decoding was dependent on learning, as CCGP did not exceed chance levels when we tested animals at an earlier time point during learning (Figure S7C), although a non-generalized linear decoder could distinguish all combinations of odors above the chance prior to learning (data not shown). The generalized decoding of a variable independent of stimulus identity has been defined as an abstract representation of that variable, in our case valence, and requires a low-dimensional representation of stimulus class in neural activity space.³¹

Dorsal CA2 activity is modulated by both social and non-social odors

To determine whether dCA2 differentially encodes social and non-social odors, we exposed mice to a set of two novel social odors (urine G and H) and two monomolecular odors (methyl butyrate and ethyl acetate) and trained them to associate one odor from each class with a water reward (Figure 6A, left). Mice learned the task with high accuracy (Figure 6A, right). An ROC analysis after learning identified subsets of cells highly selective to each of the four odors (Figure 6B), with a similar fraction of cells responding to the social and non-social odors (Figures S8A and S8B). In addition, the responses to each of the four odors were well separated in the principal component space; of particular interest, the clusters were grouped into distinct classes of social versus non-social odors and rewarded versus non-rewarded odors (Figure 6C). We trained and tested a Euclidean distance-based classifier for stimulus identity in the full vector space and found significant decoding accuracy for all four odors, time-locked to the odor onset (Figure 6D).

Dorsal CA2 encodes generalized representations of social versus non-social information

To determine whether dCA2 provides a generalized classification of social versus non-social and rewarded versus non-rewarded odors, as suggested by the PCA results, we determined the CCGP for both odor categories (Figure S9A; see also Figure S7B). When we trained an SVM binary linear classifier to discriminate the social and non-social pair of rewarded odors that same classifier decoded the distinct pair of social and non-social unrewarded odors significantly above chance (Figure 6E). Similarly, CCGP decoding was significantly above

chance when we trained a decoder to distinguish a rewarded from unrewarded social odor and tested the decoder on the pair of rewarded and unrewarded non-social odors (Figure 6F).

One straightforward implementation of generalization occurs when odor representations from individual classes tightly cluster together in activity space, resulting in a one-dimensional linear geometry. However, a geometry solely based on odor clustering within a class would lead to a low accuracy of non-generalized, within-class odor decoding.³¹ In contrast, we observed high levels of accuracy for within-class decoding of two social or two non-social odors (Figure S9B), similar to across-class decoding with a social versus non-social odor pair (Figure S9C). This implies that social and non-social odors are well separated within and between classes and that the ability to categorize odors into generalized or abstract categories likely results from a planar, two-dimensional geometry, in which the neural representations of the four odors form the vertexes of a rectangular-like spatial arrangement.³¹

We also asked whether the generalized differences in social versus non-social odor representations might be caused by the differences in arousal or odor sampling to the different classes of odors. To address this question, we compared sniff rates with social and non-social odors before and after reward learning.³² Although learning induced a reduction in sniff rate toward non-rewarded odors, we found no differences in sniff rates between social and non-social odors (Figures S10A–S10C). This finding was somewhat surprising as urine from both male and female conspecifics is normally a highly salient olfactory stimulus, eliciting a stronger exploratory response compared with monomolecular odors.³³ Indeed, when we exposed freely moving mice to a pair of filter papers imbued with the same urine and monomolecular odor samples used to monitor sniff rates, the mice preferentially explored the urine-scented paper (Figures S10D–S10F). Our finding of similar sniff rates to urine and monomolecular odors in our head-fixed task may therefore reflect habituation to the odor stimuli over the multiday course of odor-reward training.

Finally, to determine whether the generalized decoding of social versus non-social odors might reflect a simple difference in odor complexity (complex urine versus a simple monomolecular scent), we compared decoding performance using two samples of mouse urine and two samples of human urine, the latter representing a complex but behaviorally neutral odor stimulus for mice.³⁴ A binary decoder trained and tested within each odor category performed significantly above chance (Figures S11A and B). Importantly, we also observed significant CCGP levels in decoding mice from human odor classes (Figure S11C) and rewarded from unrewarded odor classes (Figure S11D). This generalized decoding did not rely on differences in the novelty of human versus mouse urine as we observed significant

(D) Left: stimulus classification accuracy of two social and two monomolecular odors plus control as a function of time (five-way Euclidean distance decoder). Shading: mean \pm 1 SD (shaded area); gray line indicates average chance decoding. Right: decoding accuracy in three individual animals (left, circles) and mean \pm 1 SD decoding (right, 0.58 ± 0.09). Chance decoding = 0.2 in this case. ***, $p < 0.001$; one-sided paired bootstrap significance test. $n = 3$ (same as in E and F). (E) CCGP for social versus monomolecular odors. Left: linear binary decoder (SVM) trained on one social/monomolecular odor pair either within the rewarded or non-rewarded category (see Figure S10A for details) and tested on the remaining odor pair. Shading: mean \pm 1 SD; gray line indicates average chance decoding. Circles: individual animal's average accuracy; bar: 0.67 ± 0.07 (mean \pm 1 SD). ***, $p < 0.001$.

(F) CCGP of rewarded versus non-rewarded odors (see also Figure 5D). Left: linear binary decoders (SVM) trained on one rewarded/non-rewarded odor pair within the social or monomolecular odor category and tested on the remaining odor pair from the excluded category. Shading: mean \pm 1 SD; gray line indicates average chance decoding. Circles: individual animal's average accuracy; bar: 0.56 ± 0.05 (mean \pm 1 SD). *, $p < 0.05$.

CCGP in an independent cohort of animals exposed to human urine-coated bedding for 2 weeks before the experiment ([Figures S11E](#) and [S11F](#)).

Dorsal CA2 contributes to the associative learning of social but not non-social odors

Given the significant correlation between dCA2 odor decoding accuracy and social odor-reward learning, we next asked whether dCA2 contributed to social odor-reward learning, using optogenetics to silence dCA2 neurons during learning. We bilaterally injected Amigo2-Cre mice with Cre-dependent AAV to express either the inhibitory opsin archaerhodopsin 3.0 (eArch3.0) or the fluorescent marker mCherry, as a control, in dCA2 PNs. We then implanted optical fibers over dCA2 to silence this region during learning ([Figures 7A](#) and [7B](#)). Only animals that showed dCA2-restricted viral expression and correct fiber placement were included in the analysis ([Figure 7C](#)).

Mice were trained by pairing one of two social odors with a water reward as described above, with dCA2 illuminated with green light (532 nm) for a total of 8 s in each 20-s-long trial of the reward learning task, starting 1 s before odor delivery. The light duration is considered safe from off-target effects, like tissue heating³⁵ ([Figure 7D](#)). Control animals readily learned the task, reaching the criterion performance by day 4 ([Figure 7E](#), left column; [Figure 7F](#)). However, in mice expressing eArch3.0 in dCA2, optogenetic silencing significantly impaired learning, with the cohort, on average, failing to reach 80% of the criterion. A fit of a logistic function to model the learning progression confirmed a significant decrease in maximal performance in eArch3.0 mice compared with controls ([Figure 7G](#)).

Silencing dCA2 caused an even greater impairment in learning when we restricted our analysis to the initial trials of each training session on a given day ([Figure 7E](#)) and focused on the learning to withhold licking to unrewarded odor B, which was more difficult for mice than learning to lick to rewarded odor A. For such trials, dCA2 silencing produced a profound delay in the ability of mice to learn to withhold licking to the unrewarded odor, with a significant rightward shift of the midpoint of a logistic fit to the learning curve³⁶ ([Figure 7G](#)). The greater impairment in response to dCA2 silencing in performance in the early trials of a session, when mice needed to recall the memory of the task contingency from the previous day's session, is consistent with the role of the hippocampus in long-term associative memory.²

As previous studies have found that dCA2 is required for social memory but is less critical for forms of non-social hippocampal-dependent memory, we next asked whether dCA2 was also required for learning the association between reward and a non-social odor. We first used a pair of human urines as non-social odors with a high degree of molecular complexity. We again trained mice expressing either eArch3.0 or mCherry in dCA2 in the odor-reward association task and illuminated dCA2 during learning. In contrast to the impact on social odor-reward learning, optogenetic inhibition of dCA2 failed to impair reward learning with the human odors ([Figure S12](#)). Optogenetic silencing of dCA2 also failed to impair learning with two monomolecular non-social odors ([Figure S12](#)).

The greater role of dCA2 in social compared with non-social odor-reward learning was also apparent at the level of dCA2

PN odor responses. Thus, although social odor-reward learning enhanced dCA2 social odor discrimination as noted above ([Figure 4](#)), odor-reward learning with two monomolecular did not enhance their discrimination by dCA2 activity. This lack of change in dCA2 neuron non-social odor discrimination was observed both at the single-cell level of dCA2 PN odor selectivity, based on ROC analysis, and at the population level, based on SVM decoding ([Figure S13](#)).

DISCUSSION

Similar to the well-described hippocampal place cells that encode spatial location soon after an animal enters a new environment,^{37,38} here, we found for the first time subsets of dCA2 PNs that selectively responded to novel social odors soon after their initial presentation, thereby encoding individual-specific representations. As social memory in rodents, which is typically assessed by the discrimination of a novel from a familiar individual, depends on olfactory cues,^{7,39} these representations of social odor are likely to provide a mechanism by which dCA2 contributes to social novelty recognition memory.^{12–14}

However, social episodic memory extends beyond the discrimination of social novelty and requires the association of a given conspecific with a specific social experience, including its positive or negative valence. Our findings that dCA2 was required for social odor-reward learning and that dCA2 social odor representations were refined by experience in an associative reward-learning task—leading to an increased discriminability of rewarded from unrewarded social odors—provide the first evidence that dCA2 participates in forms of social memory that are more complex than social novelty detection. Such results are consistent with the view that dCA2 may enable the association of an individual with a rewarding or aversive experience. Indeed, the ability of dCA2 to incorporate social information with past experience may contribute to its role in regulating social aggression.⁴⁰

There are computational advantages for the brain to enact a compromise between persistence and flexibility,^{41–43} and dCA2 seems to strike this balance for social odor recognition. Thus, although learning refined dCA2 social odor representations, stimulus identity could be reliably decoded across at least 2 days, even across a change of reward contingency. In this way, a consistent representation of the identity of an individual can be maintained across differing experiences.

One key question about the function of dCA2 is the extent to which it is specialized for social memory. Previous studies have shown that dCA2 is required for the detection of social novelty but not for the detection of a novel object.¹² Here, we found that although dCA2 contributed to social odor-reward learning, it did not contribute to non-social odor-reward learning. Similarly, we found that although dCA2 could discriminate pairs of social and non-social odors, only the social odor representations were enhanced by odor-reward learning.

Further evidence that dCA2 differentially processes social and non-social odors came from our finding that dCA2 population activity provided a generalized or “abstract” classification of social versus non-social odors independent of the specific odor identity. Following Bernardi et al.,³¹ representations were

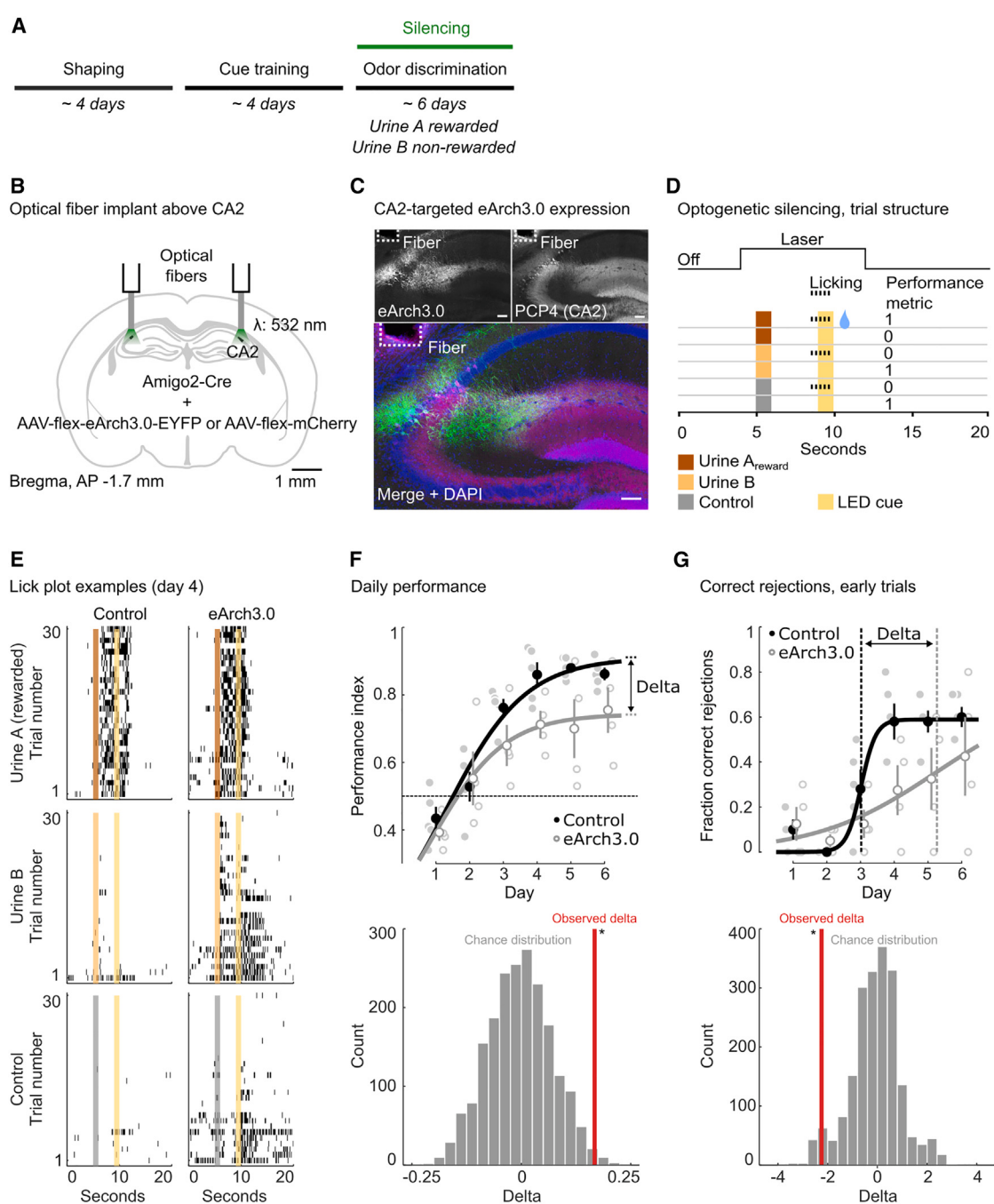


Figure 7. Optogenetic silencing of dCA2 impairs the learning of social odor-reward associations

- (A) Timeline of experiment testing effect of optogenetic silencing of dCA2 on social odor-reward learning (see **STAR Methods** for details).
- (B) Schematic of optic fiber implant above dCA2 region expressing eArch3.0 or mCherry control.
- (C) Post hoc confocal images of eArch3.0 expression counterstained with a marker for dCA2 (PCP4). Scale bars: 100 μm.
- (D) Schematic of the experimental paradigm. In a given trial, green laser light was provided starting 1 s before odor onset until 2 s after the cue window/reward presentation (total of 8 per 20 s trial). Both groups of mice performed 90 trials per session, 30 trials per stimulus.
- (E) Example lick plots on day 4 of training. Randomly presented odors are re-arranged according to their odor-class and plotted as a block within a column.
- (F) Social odor-reward learning for eArch3.0 and mCherry control groups. Upper: the performance of individual animals (controls: small filled gray circles; eArch3.0: small open circles) as a function of training day. Larger circles: mean ± SEM values. Line: three-parameter logistic regression model. The significance of the difference between the maximal performance levels (control: 0.9; eArch3.0: 0.7) of the fitted models (delta) is determined using a permutation test (lower); *, p < 0.05. n = 5 and 4 for controls and eArch3.0 expressing mice, respectively.
- (G) Fraction of correct rejections in the first 30 trials of a given session. The midpoint of the logistic model is significantly shifted to later days in the eArch3.0 expressing group (control: 2.0 days; eArch3.0: 5.3 days). Lower panel as in (F). *, p < 0.05.

defined as generalized or abstract based on the ability of a linear classifier trained on one pair of stimuli from social and non-social odor classes to accurately decode odor class when tested on a second pair of distinct stimuli from the same two classes. Such generalized decoding implies that dCA2 odor representations adopt a low-dimensional geometric arrangement in neural activity space.

In the simplest case, low-dimensional representations can occur when odors within a class are tightly clustered in neural activity space.³¹ In this case, the neural responses to the two classes of stimuli will form two clusters of points along a one-dimensional line. Thus, a linear classifier trained to distinguish one pair of social/non-social odors would be able to decode a second pair of social/non-social odors. However, such a tight clustering would make it difficult to decode pairs of odors in the same class, owing to the proximity of their neural representations. Our finding of highly accurate within-class decoding of both social and non-social odors is incompatible with a tightly clustered linear geometry but suggests that the responses to the pairs of social and non-social odors are represented in a low-dimensional rectangular-like planar geometry, with the social and non-social odors arrayed along parallel edges of the rectangle. This allows both generalized decoding, as a classifier plane that separates one pair of social/non-social odors will also separate the other pair (because of the rectangular arrangement), and high within-class decoding because odor pairs within a class can be well separated from one across one edge of the rectangle.

Several questions remain about the neural mechanisms by which dCA2 encodes social information into structured representations of stimulus class and how these representations are modified by learning. The generalized classification of social compared with non-social odors must ultimately depend on differences in the sensory qualities of the odorants in the social and non-social classes. Whether dCA2 computes this odor classification locally or whether it is inherited from dCA2 inputs remains to be determined. It is also unclear as to how dCA2 selectively participates in social odor learning, although a likely candidate is provided by its highly enriched expression of receptors for social neuropeptides, including the AVPR1b receptor for arginine vasopressin⁴⁴ and the receptor for oxytocin,^{45,46} which regulate dCA2 intrinsic excitability and synaptic inputs^{47–49} and contribute to social memory.^{18,44,45,50} It will also be of interest to study a wider range of social odor responses, including male versus female social odors, social odors from different mouse strains, and the role of social odor processing in social interactions in freely behaving mice. Studies exploring these questions, in both wild-type mice and mouse disease models, may provide further mechanistic insights into social information processing in dCA2 and as to how this may be disrupted in neuropsychiatric disorders associated with abnormal social cognition.⁵¹

STAR★METHODS

Detailed methods are provided in the online version of this paper and include the following:

● KEY RESOURCES TABLE

● RESOURCE AVAILABILITY

- Lead contact
- Materials availability
- Data and code availability

● EXPERIMENTAL MODEL AND SUBJECT DETAILS

● METHOD DETAILS

- Stereotaxic viral delivery
- Surgical implants
- Immunohistochemistry
- Odor selection
- Behavioral setup
- Behavioral training
- Two-photon calcium imaging
- Odor exploration in freely moving animals

● QUANTIFICATION AND STATISTICAL ANALYSIS

- Signal extraction
- Longitudinal registration
- Data processing
- Respiration sampling
- Data analysis
- ROC analysis
- PCA analysis
- Decoder analysis
- Fisher's Exact Test
- Logistic model
- Trajectory analysis and analysis of odor exploration time

SUPPLEMENTAL INFORMATION

Supplemental information can be found online at <https://doi.org/10.1016/j.neuron.2023.04.026>.

ACKNOWLEDGMENTS

We thank Darcy Peterka, Jennifer Bussell, Teddy G. Goetz, Clay O. Lacefield, Kevin Bolding, and Andrew Fink for their help with the experimental setup; Andres Villegas for help implementing video-based animal tracking; Rafaela Morais-Ribeiro for help scoring behavioral videos; Walter Fischler-Ruiz, Daniel Salzman, Stefano Fusi, Arjun V. Masurkar, and Lara Boyle for critical comments on the manuscript; Alex H. Williams, Lorenzo Posani, Franziska Auer, and the Siegelbaum laboratory for helpful discussions; and the Research Instrumentation Core at Zuckerman Institute. This work was supported by a NARSAD Brain and Behavior Research Young Investigator Award (S.I.H.), grants R01 MH104602 and R01 MH106629 from the National Institute of Mental Health (S.A.S), and a grant from the Zegar Family Foundation (S.A.S.).

AUTHOR CONTRIBUTIONS

S.I.H. and S.A.S. conceived the project and wrote the manuscript. S.I.H. built the experimental setup, and S.I.H. and S.B. designed and performed the imaging experiments. S.B. performed optogenetic experiments and experiments on freely moving mice and helped edit the manuscript. S.I.H. wrote analysis scripts and analyzed the data.

DECLARATION OF INTERESTS

The authors declare no competing interests.

INCLUSION AND DIVERSITY

We support inclusive, diverse, and equitable conduct of research.

Received: September 28, 2021

Revised: October 25, 2022

Accepted: April 21, 2023

Published: May 15, 2023

REFERENCES

1. Scoville, W.B., and Milner, B. (1957). Loss of recent memory after bilateral hippocampal lesions. *J. Neurol. Neurosurg. Psychiatry* 20, 11–21. <https://doi.org/10.1136/jnnp.20.1.11>.
2. Eichenbaum, H. (2017). Memory: organization and control. *Annu. Rev. Psychol.* 68, 19–45. <https://doi.org/10.1146/annurev-psych-010416-044131>.
3. Kogan, J.H., Frankland, P.W., and Silva, A.J. (2000). Long-term memory underlying hippocampus-dependent social recognition in mice. *Hippocampus* 10, 47–56. [https://doi.org/10.1002/\(SICI\)1098-1063\(2000\)10:1<47::AID-HIPO5>3.0.CO;2-6](https://doi.org/10.1002/(SICI)1098-1063(2000)10:1<47::AID-HIPO5>3.0.CO;2-6).
4. Sanders, H.I., and Warrington, E.K. (1971). Memory for remote events in amnesic patients. *Brain* 94, 661–668. <https://doi.org/10.1093/brain/94.4.661>.
5. Sliwa, J., Planté, A., Duhamel, J.R., and Wirth, S. (2016). Independent neuronal representation of facial and vocal identity in the monkey hippocampus and inferotemporal cortex. *Cereb. Cortex* 26, 950–966. <https://doi.org/10.1093/cercor/bhu257>.
6. Uekita, T., and Okanoya, K. (2011). Hippocampus lesions induced deficits in social and spatial recognition in Octodon degus. *Behav. Brain Res.* 219, 302–309. <https://doi.org/10.1016/j.bbr.2011.01.042>.
7. Hurst, J.L., Payne, C.E., Nevison, C.M., Marie, A.D., Humphries, R.E., Robertson, D.H.L., Cavaggioni, A., and Beynon, R.J. (2001). Individual recognition in mice mediated by major urinary proteins. *Nature* 414, 631–634. <https://doi.org/10.1038/414631a>.
8. Brennan, P.A., and Kendrick, K.M. (2006). Mammalian social odours: attraction and individual recognition. *Philos. Trans. R. Soc. Lond. B Biol. Sci.* 361, 2061–2078. <https://doi.org/10.1098/rstb.2006.1931>.
9. Igarashi, K.M., Lu, L., Colgin, L.L., Moser, M.B., and Moser, E.I. (2014). Coordination of entorhinal–hippocampal ensemble activity during associative learning. *Nature* 510, 143–147. <https://doi.org/10.1038/nature13162>.
10. Li, Y., Xu, J., Liu, Y., Zhu, J., Liu, N., Zeng, W., Huang, N., Rasch, M.J., Jiang, H., Gu, X., et al. (2017). A distinct entorhinal cortex to hippocampal CA1 direct circuit for olfactory associative learning. *Nat. Neurosci.* 20, 559–570. <https://doi.org/10.1038/nn.4517>.
11. Woods, N.I., Stefanini, F., Apodaca-Montano, D.L., Tan, I.M.C., Biane, J.S., and Kheirbek, M.A. (2020). The dentate gyrus classifies cortical representations of learned stimuli. *Neuron* 107, 173–184.e6. <https://doi.org/10.1016/j.neuron.2020.04.002>.
12. Hitti, F.L., and Siegelbaum, S.A. (2014). The hippocampal CA2 region is essential for social memory. *Nature* 508, 88–92. <https://doi.org/10.1038/nature13028>.
13. Stevenson, E.L., and Caldwell, H.K. (2014). Lesions to the CA2 region of the hippocampus impair social memory in mice. *Eur. J. Neurosci.* 40, 3294–3301. <https://doi.org/10.1111/ejn.12689>.
14. Meira, T., Leroy, F., Buss, E.W., Oliva, A., Park, J., and Siegelbaum, S.A. (2018). A hippocampal circuit linking dorsal CA2 to ventral CA1 critical for social memory dynamics. *Nat. Commun.* 9, 4163. <https://doi.org/10.1038/s41467-018-06501-w>.
15. Oliva, A., Fernández-Ruiz, A., Leroy, F., and Siegelbaum, S.A. (2020). Hippocampal CA2 sharp-wave ripples reactivate and promote social memory. *Nature* 587, 264–269. <https://doi.org/10.1038/s41586-020-2758-y>.
16. Leroy, F., Brann, D.H., Meira, T., and Siegelbaum, S.A. (2017). Input-timing-dependent plasticity in the hippocampal CA2 region and its potential role in social memory. *Neuron* 95, 1089–1102.e5. <https://doi.org/10.1016/j.neuron.2017.07.036>.
17. Leroy, F., de Solis, C.A., Boyle, L.M., Bock, T., Lofaro, O.M., Buss, E.W., Asok, A., Kandel, E.R., and Siegelbaum, S.A. (2022). Enkephalin release from VIP interneurons in the hippocampal CA2/3a region mediates heterosynaptic plasticity and social memory. *Mol. Psychiatry* 27, 2879–2900. <https://doi.org/10.1038/s41380-021-01124-y>.
18. Smith, A.S., Williams Avram, S.K., Cymerblit-Sabba, A., Song, J., and Young, W.S. (2016). Targeted activation of the hippocampal CA2 area strongly enhances social memory. *Mol. Psychiatry* 21, 1137–1144. <https://doi.org/10.1038/mp.2015.189>.
19. Chen, S., He, L., Huang, A.J.Y., Boehringer, R., Robert, V., Wintzer, M.E., Polygalov, D., Weitemier, A.Z., Tao, Y., Gu, M., et al. (2020). A hypothalamic novelty signal modulates hippocampal memory. *Nature* 586, 270–274. <https://doi.org/10.1038/s41586-020-2771-1>.
20. Donegan, M.L., Stefanini, F., Meira, T., Gordon, J.A., Fusi, S., and Siegelbaum, S.A. (2020). Coding of social novelty in the hippocampal CA2 region and its disruption and rescue in a 22q11.2 microdeletion mouse model. *Nat. Neurosci.* 23, 1365–1375. <https://doi.org/10.1038/s41593-020-00720-5>.
21. Okuyama, T., Kitamura, T., Roy, D.S., Itohara, S., and Tonegawa, S. (2016). Ventral CA1 neurons store social memory. *Science* 353, 1536–1541. <https://doi.org/10.1126/science.aaf7003>.
22. Alexander, G.M., Farris, S., Pirone, J.R., Zheng, C., Colgin, L.L., and Dudek, S.M. (2016). Social and novel contexts modify hippocampal CA2 representations of space. *Nat. Commun.* 7, 10300. <https://doi.org/10.1038/ncomms10300>.
23. Chen, T.W., Wardill, T.J., Sun, Y., Pulver, S.R., Renninger, S.L., Baohan, A., Schreiter, E.R., Kerr, R.A., Orger, M.B., Jayaraman, V., et al. (2013). Ultrasensitive fluorescent proteins for imaging neuronal activity. *Nature* 499, 295–300. <https://doi.org/10.1038/nature12354>.
24. Dombeck, D.A., Harvey, C.D., Tian, L., Looger, L.L., and Tank, D.W. (2010). Functional imaging of hippocampal place cells at cellular resolution during virtual navigation. *Nat. Neurosci.* 13, 1433–1440. <https://doi.org/10.1038/nn.2648>.
25. Green, D.M., and Swets, J.A. (1966). *Signal Detection Theory and Psychophysics* (John Wiley).
26. Najafi, F., Elsayed, G.F., Cao, R., Pnevmatikakis, E., Latham, P.E., Cunningham, J.P., and Churchland, A.K. (2020). Excitatory and inhibitory subnetworks are equally selective during decision-making and emerge simultaneously during learning. *Neuron* 105, 165–179.e8. <https://doi.org/10.1016/j.neuron.2019.09.045>.
27. Hofmann, T., Schölkopf, B., and Smola, A.J. (2008). Kernel methods in machine learning. *Ann. Statist.* 36, 1171–1220. <https://doi.org/10.1214/009053607000000677>.
28. Stefanini, F., Kushnir, L., Jimenez, J.C., Jennings, J.H., Woods, N.I., Stuber, G.D., Kheirbek, M.A., Hen, R., and Fusi, S. (2020). A distributed neural code in the dentate gyrus and in CA1. *Neuron* 107, 703–716.e4. <https://doi.org/10.1016/j.neuron.2020.05.022>.
29. Sheintuch, L., Rubin, A., Brande-Eilat, N., Geva, N., Sadeh, N., Pinchasof, O., and Ziv, Y. (2017). Tracking the same neurons across multiple days in Ca2+ imaging data. *Cell Rep.* 21, 1102–1115. <https://doi.org/10.1016/j.celrep.2017.10.013>.
30. Feierstein, C.E., Quirk, M.C., Uchida, N., Sosulski, D.L., and Mainen, Z.F. (2006). Representation of spatial goals in rat orbitofrontal cortex. *Neuron* 51, 495–507. <https://doi.org/10.1016/j.neuron.2006.06.032>.
31. Bernardi, S., Benna, M.K., Rigotti, M., Munuera, J., Fusi, S., and Salzman, C.D. (2020). The geometry of abstraction in the hippocampus and prefrontal cortex. *Cell* 183, 954–967.e21. <https://doi.org/10.1016/j.cell.2020.09.031>.
32. Jordan, R., Fukunaga, I., Kollo, M., and Schaefer, A.T. (2018). Active sampling state dynamically enhances olfactory bulb odor representation. *Neuron* 98, 1214–1228.e5. <https://doi.org/10.1016/j.neuron.2018.05.016>.
33. Levy, D.R., Tamir, T., Kaufman, M., Parabucki, A., Weissbrod, A., Schneidman, E., and Yizhar, O. (2019). Dynamics of social representation

- in the mouse prefrontal cortex. *Nat. Neurosci.* 22, 2013–2022. <https://doi.org/10.1038/s41593-019-0531-z>.
34. Rivard, G.F., Moser, E.G., D'Ambrose, S.P., and Lin, D.M. (2014). Lack of fear response in mice (*Mus musculus*) exposed to human urine odor. *J. Am. Assoc. Lab. Anim. Sci.* 53, 141–145.
 35. Trouche, S., Perestenko, P.V., van de Ven, G.M., Bratley, C.T., McNamara, C.G., Campo-Urriza, N., Black, S.L., Reijmers, L.G., and Dupret, D. (2016). Recoding a cocaine-place memory engram to a neutral engram in the hippocampus. *Nat. Neurosci.* 19, 564–567. <https://doi.org/10.1038/nn.4250>.
 36. Park, A.J., Harris, A.Z., Martyniuk, K.M., Chang, C.Y., Abbas, A.I., Lowes, D.C., Kellendonk, C., Gogos, J.A., and Gordon, J.A. (2021). Reset of hippocampal–prefrontal circuitry facilitates learning. *Nature* 591, 615–619. <https://doi.org/10.1038/s41586-021-03272-1>.
 37. O'Keefe, J., and Burgess, N. (2017). The hippocampus as a spatial map. Preliminary evidence from unit activity in the freely-moving rat. *Brain Res.* 34, 171–175. [https://doi.org/10.1016/0006-8993\(71\)90358-1](https://doi.org/10.1016/0006-8993(71)90358-1).
 38. Leutgeb, S., Leutgeb, J.K., Treves, A., Moser, M.B., and Moser, E.I. (2004). Distinct ensemble codes in hippocampal areas CA3 and CA1. *Science* 305, 1295–1298. <https://doi.org/10.1126/science.1100265>.
 39. Thom, M.D., and Hurst, J.L. (2004). Individual recognition by scent. *Ann. Zool. Fennici.* 41, 765–787.
 40. Leroy, F., Park, J., Asok, A., Brann, D.H., Meira, T., Boyle, L.M., Buss, E.W., Kandel, E.R., and Siegelbaum, S.A. (2018). A circuit from hippocampal CA2 to lateral septum disinhibits social aggression. *Nature* 564, 213–218. <https://doi.org/10.1038/s41586-018-0772-0>.
 41. Mau, W., Hasselmo, M.E., and Cai, D.J. (2020). The brain in motion: how ensemble fluidity drives memory-updating and flexibility. *eLife* 9, e63550. <https://doi.org/10.7554/eLife.63550>.
 42. Richards, B.A., and Frankland, P.W. (2017). The persistence and transience of memory. *Neuron* 94, 1071–1084. <https://doi.org/10.1016/j.neuron.2017.04.037>.
 43. Rule, M.E., O'Leary, T., and Harvey, C.D. (2019). Causes and consequences of representational drift. *Curr. Opin. Neurobiol.* 58, 141–147. <https://doi.org/10.1016/j.conb.2019.08.005>.
 44. Young, W.S., Li, J., Wersinger, S.R., and Palkovits, M. (2006). The vasopressin 1b receptor is prominent in the hippocampal area CA2 where it is unaffected by restraint stress or adrenalectomy. *Neuroscience* 143, 1031–1039. <https://doi.org/10.1016/j.neuroscience.2006.08.040>.
 45. Raam, T., McAvoy, K.M., Besnard, A., Veenema, A.H., and Sahay, A. (2017). Hippocampal oxytocin receptors are necessary for discrimination of social stimuli. *Nat. Commun.* 8, 2001. <https://doi.org/10.1038/s41467-017-02173-0>.
 46. Mitre, M., Marlin, B.J., Schiavo, J.K., Morina, E., Norden, S.E., Hackett, T.A., Aoki, C.J., Chao, M.V., and Froemke, R.C. (2016). A distributed network for social cognition enriched for oxytocin receptors. *J. Neurosci.* 36, 2517–2535. <https://doi.org/10.1523/JNEUROSCI.2409-15.2016>.
 47. Pagani, J.H., Zhao, M., Cui, Z., Avram, S.K., Caruana, D.A., Dudek, S.M., and Young, W.S. (2015). Role of the vasopressin 1b receptor in rodent aggressive behavior and synaptic plasticity in hippocampal area CA2. *Mol. Psychiatry* 20, 490–499. <https://doi.org/10.1038/mp.2014.47>.
 48. Liu, J.J., Eyring, K.W., König, G.M., Kostenis, E., and Tsien, R.W. (2022). Oxytocin-modulated ion channel ensemble controls depolarization, integration and burst firing in CA2 pyramidal neurons. *J. Neurosci.* 42, 7707–7720. <https://doi.org/10.1523/JNEUROSCI.0921-22.2022>.
 49. Tirko, N.N., Eyring, K.W., Carcea, I., Mitre, M., Chao, M.V., Froemke, R.C., and Tsien, R.W. (2018). Oxytocin transforms firing mode of CA2 hippocampal neurons. *Neuron* 100, 593–608.e3. <https://doi.org/10.1016/j.neuron.2018.09.008>.
 50. Lin, Y.T., Hsieh, T.Y., Tsai, T.C., Chen, C.C., Huang, C.C., and Hsu, K.S. (2018). Conditional deletion of hippocampal CA2/CA3a oxytocin receptors impairs the persistence of long-term social recognition memory in mice. *J. Neurosci.* 38, 1218–1231. <https://doi.org/10.1523/JNEUROSCI.1896-17.2017>.
 51. Chevaleyre, V., and Piskorowski, R.A. (2016). Hippocampal area CA2: an overlooked but promising therapeutic target. *Trends Mol. Med.* 22, 645–655. <https://doi.org/10.1016/j.molmed.2016.06.007>.
 52. Schindelin, J., Arganda-Carreras, I., Frise, E., Kaynig, V., Longair, M., Pietzsch, T., Preibisch, S., Rueden, C., Saalfeld, S., Schmid, B., et al. (2012). Fiji: an open-source platform for biological-image analysis. *Nat. Methods* 9, 676–682. <https://doi.org/10.1038/nmeth.2019>.
 53. Pachitariu, M., Stringer, C., Dipoppa, M., Schröder, S., Rossi, L.F., Dalgleish, H., Carandini, M., and Harris, K.D. (2017). Suite2p: beyond 10,000 neurons with standard two-photon microscopy. Preprint at bioRxiv. <https://doi.org/10.1101/061507>.
 54. Lauer, J., Zhou, M., Ye, S., Menegas, W., Schneider, S., Nath, T., Rahman, M.M., Di Santo, V., Soberanes, D., Feng, G., et al. (2022). Multi-animal pose estimation, identification and tracking with DeepLabCut. *Nat. Methods* 19, 496–504. <https://doi.org/10.1038/s41592-022-01443-0>.
 55. Friard, O., and Gamba, M. (2016). BORIS: a free, versatile open-source event-logging software for video/audio coding and live observations. *Methods Ecol. Evol.* 7, 1325–1330. <https://doi.org/10.1111/2041-210X.12584>.
 56. Bolding, K.A., and Franks, K.M. (2017). Complementary codes for odor identity and intensity in olfactory cortex. *eLife* 6, e22630. <https://doi.org/10.7554/eLife.22630>.
 57. Stringer, C., and Pachitariu, M. (2019). Computational processing of neural recordings from calcium imaging data. *Curr. Opin. Neurobiol.* 55, 22–31. <https://doi.org/10.1016/j.conb.2018.11.005>.
 58. Mackevicius, E.L., Bahle, A.H., Williams, A.H., Gu, S., Denisenko, N.I., Goldman, M.S., and Fee, M.S. (2019). Unsupervised discovery of temporal sequences in high-dimensional datasets, with applications to neuroscience. *eLife* 8, e38471. <https://doi.org/10.7554/eLife.38471>.
 59. Chang, C.-C., and Lin, C.-J. (2011). LIBSVM: a library for support vector machines. *ACM Trans. Intell. Syst. Technol.* 2, 1–27. <https://doi.org/10.1145/1961189.1961199>.
 60. Efron, B., and Tibshirani, R.J. (1993). *An Introduction to the Bootstrap*, First Edition (Chapman and Hall/CRC).
 61. North, B.V., Curtis, D., and Sham, P.C. (2002). A note on the calculation of empirical P values from Monte Carlo procedures. *Am. J. Hum. Genet.* 71, 439–441.

STAR★METHODS

KEY RESOURCES TABLE

REAGENT or RESOURCE	SOURCE	IDENTIFIER
Antibodies		
Rabbit polyclonal anti-PCP4	Sigma-Aldrich	Cat#HPA005792; RRID: AB_1855086
Bacterial and virus strains		
AAV2/1-EF1a-DIO-GCaMP6s-P2A-nls-dTomato	Addgene (Jonathan Ting)	RRID: Addgene_51082
AAV2/2-EF1a-DIO-mCherry	Addgene (Bryan Roth)	RRID: Addgene_50462
AAV2/2-EF1a-DIO-eArch3.0-eYFP	UNC Vector Core	N/A
Biological samples		
Mouse urine samples, C57BL6, male (~12 weeks)	BiolVT	Cat#MSE01URINEMNN
Human urine samples, male (~20 years)	BiolVT	Cat#HUMANURINEMNN
Critical commercial assays		
Mouse Creatinine Assay Kit	CrystalChem	Cat#80350
Experimental models: Organisms/strains		
B6.Cg-Tg(Amigo2-cre)1Sieg/J	Hitti and Siegelbaum ¹²	RRID: IMSR_JAX:030215
Software and algorithms		
Fiji	Schindelin et al. ⁵²	https://imagej.net/software/fiji/
MATLAB R2020b	MathWorks	https://www.mathworks.com/products/matlab.html
Scanimate 5.6	Vidrio	https://vidriotechnologies.com/download-scanimate/
Suite2p	Pachitariu et al. ⁵³	https://github.com/cortex-lab/Suite2P
DeepLabCut	Lauer et al. ⁵⁴	https://deeplabcut.github.io/DeepLabCut/README.html
BORIS	Friard and Gamba ⁵⁵	https://www.boris.unito.it/

RESOURCE AVAILABILITY

Lead contact

Further information and requests for resources and reagents should be directed to and will be fulfilled by the lead contact Steven A. Siegelbaum (sas8@columbia.edu).

Materials availability

This study did not generate new reagents.

Data and code availability

Data, code, and any additional information required to reanalyze the data reported in this paper is available from the [lead contact](#) upon request.

EXPERIMENTAL MODEL AND SUBJECT DETAILS

All mouse procedures were performed in accordance with the NIH guidelines and with the approval of the Columbia University Institutional Animal Care and Use Committee. We used heterozygous, sexually naïve Amigo2-Cre,¹² three to six month old female mice, except for experiments including human urine samples, where we used a mixed group of male and females (no qualitative difference in behavioral performance between genders was apparent in this group), all on the C57Bl/6J background (The Jackson Laboratory). Mice were maintained on a 12-h light-dark cycle with ad libitum access to food. For behavioral training and imaging, mice were kept on a water schedule; they received 1 ml in total per day. Health was monitored daily, and we gave additional water if body weight fell below 80% of the pre-schedule weight. Mice were housed in groups of two to four.

METHOD DETAILS

Stereotaxic viral delivery

For imaging experiments, mice were injected with a bicistronic Cre-dependent AAV2/1 expressing the genetically encoded activity indicator GCaMP6s and nuclear tdTomato, the latter serving as a structural marker to improve motion correction.

AAV-EF1a-DIO-GCaMP6s-P2A-nls-dTomato was a gift from Jonathan Ting (Addgene viral prep #51082-AAV1; <http://n2t.net/addgene:51082>; RRID: Addgene_51082). Injections were targeted unilaterally to the left dorsal CA2 region using Allen Brain Atlas coordinates: anterior-posterior (AP): -1.7, medial-lateral (ML): 2.0, from bregma; dorsal-ventral (DV): -1.3 from pia mater. ~60 nl in saline diluted virus (titer: 1×10^{12} gc/ml) were delivered at 1 nl s⁻¹ using pressure injection. A cranial window was implanted 24h after injections.

In silencing experiments, AAV2/2-EF1a-DIO-eArch3.0-eYFP (titer: 4.0×10^{12} gc/ml) or AAV2/2-EF1a-DIO-mCherry (titer: 4.4×10^{12} gc/ml) was bilaterally injected (200 nl per site) to express the inhibitory opsin eArch3.0 or a fluorescent control selectively in dCA2. Right after injections, optogenetic fibers were implanted.

Surgical implants

Mice were implanted with an imaging window (diameter 3 mm, height 1.8 mm) over the left dorsal hippocampus and a custom stainless-steel head-post to allow for head-fixation during imaging. Imaging cannulas were constructed by adhering (Norland optical adhesive) a 3 mm glass coverslip (Warner instruments) to the steel cannula (Ziggy's tubes and wires). For the implant, mice were anesthetized (isoflurane) and provided with anti-inflammatory (dexamethasone 2 mg/kg, s.c.) and analgesic (buprenorphine SR, 1mg/kg, s.c.) treatment. A single 3 mm craniotomy, centered at the site of injection, was performed using a trephine drill. Cortex was irrigated using ice cold sterile saline supplemented with 3 mM MgCl₂ and 1 mM CaCl₂ and carefully removed through vacuum aspiration to allow visual access to the hippocampus. The prepared optic cannula was inserted at a 15° angle and secured with acrylic-based adhesive (Vetbond, 3M). Both cannula and head-post were then permanently fixed to the skull using dental cement (Metabond, Parkell). Mice recovered in their home cage, and behavioral training started two weeks after surgery.

Optical fiber assemblies (200 um core, 0.37 NA, 3 mm, RWD Life Science Inc.) were implanted at the site of injections and placed on top of the alveus. Fibers were permanently fixed using dental cement.

Immunohistochemistry

Post hoc immunostaining of brain sections were performed as previously reported.⁴⁰ Briefly, mice were perfused with chilled 4% PFA in PBS. 60 µm coronal sections were prepared and area dCA2 was counterstained using rabbit anti-PCP4 (1:400, Sigma-Aldrich, #HPA005792).

Odor selection

Urine samples from individual male mice (1-3 ml, from ~three-month-old animals) and humane urine samples (male, 20-30 years old) were commercially ordered (BioIVT). Samples arrived frozen and were divided into aliquots of 100 µl upon arrival and stored at -20°C until their final use. We tested the concentration of creatinine in some urine samples (Mouse Creatinine Assay Kit; CrystalChem) as an indicator for potential large differences in the degree of concentration but found only minor variability (15 mg/dl ± 3; mean ± SD). For experiments, aliquots were diluted in water (1:50) and kept in 22 ml amber glass screw cap vials sealed with a PTFE/silicone septum (Supelco). Dilutions were kept during independent experimental phases and cohorts and stored over night at 4°C.

Ethyl acetate, methyl butyrate (1:200 and 1:2000, respectively; Sigma-Aldrich), eugenol, and propyl propionate (both 10%; TCI) were diluted in mineral oil.

Behavioral setup

A custom eight-channel olfactometer was built and controlled using custom written MATLAB (MathWorks, R2020b) code. A constant stream of 1 l/min medical air and a second, independent carrier stream (0.5 l/min) were combined at a nose cone, which was placed 0.5 cm in front of the head-fixed animal's nose. The carrier line had either air that was guided over individual reservoir bottles containing the respective odors or simple water as blank control. A microcontroller-controlled (Arduino) valve array (The Lee Company) switched precisely between blank and odor bottles, which resulted in a total air stream of 1.5 l/min across a session. For odor-sampling experiments the nose piece was replaced by a 4-way custom-printed stainless steel piece.⁵⁶ One opening was directed at the animal's nose. An airflow sensor (AWM3300V, Honeywell) was placed at the opposing site and its voltage output was sampled at 500 Hz. Air stream in- and outlet were arranged perpendicular to the sniff direction. The water-delivery system consisted of a valve-controlled, gravity-driven water supply that was connected to a 22G gavage needle, which was held in place ~3mm in front of the animal's mouth. A capacitance sensor (Sparkfun, #AT42QT1010) was soldered onto the needle to register lick behavior. The sampling rate was set to 20 Hz. A white LED, which indicated the cue window, was placed ~4 cm in front and slightly above the animal's head. To synchronize the behavioral setup with the two-photon image acquisition, both the microscope and the olfactometer were set to send TTL pulses continuously to a master data acquisition board (National Instruments, #USB-6001), which sampled at 500 Hz.

Behavioral training

Throughout an experiment, mice were head-fixed in a custom-printed enclosure which prevented larger movements but provided enough space for animals to adjust their posture. Mice were initially habituated to be head-fixed by just placing them repeatedly in the enclosure until they showed no obvious sign of discomfort (e.g., agitation). In all following phases, at the start of each session, the animal was head-fixed and kept in the set-up for ~10 min without odor presentation to habituate to the set-up and mitigate transport induced stress. In sessions that included the association of an odor with a water reward delivery, the amount of water received during

the task was registered and the difference to the 1 ml/day water schedule was provided to the animal in a dish placed in a separate cage after training. In the initial ‘shaping’ phase, mice were trained to associate a light cue with water delivery (4 μ l) through the lick port. The protocol for this phase consisted of 20 unconditional trials, where a five-seconds-long baseline was followed by a one-second LED cue. After the cue, a water droplet was delivered. The 20 unconditional trials were followed by a maximum of 80 conditional trials, where the five-second baseline was followed by the LED cue, however, now the animal had to actively engage by licking at the lick spout to immediately trigger a water reward. If the mouse did not lick within four seconds, during which the LED was continuously on, the trial was considered a failed trial and a new trial was started. A maximum of 200 attempts were carried out on a single day. Once the animal consistently reached 80 success trial in 80 attempts, the animal moved to the ‘cue-training’ phase. Here, a single trial lasted ten seconds. An eight-seconds-long baseline was followed by a one-second-long LED cue, in which the animal had to actively lick at the lick spout. If it did, it received a water reward right after the cue window and a new trial was started. If it failed, no punishment was imposed upon the animal and the new trial was started. The animal had to complete 100 trials per session and the performance was monitored as the fraction of successful trials over all trials. Once the animal performed > 80% correct trials, the animal moved to the actual ‘odor-discrimination’ phase. In this phase a single trial lasted 20 seconds: a five-seconds baseline, a one-second odor/blank presentation, a three-seconds delay, a one-second cue-window, and a ten-seconds inter-trial-interval. Depending on the paradigm (two or four odor discrimination), one or two odors were paired with a reward, and the mouse had to actively lick at the spout during the cue-window after those odors were presented, but not to the others. Licking after the correct odors and withholding to the non-rewarded odors or blank trials, was counted as a correct trial and the performance measure was the fraction of correct trials over all trials. Mice underwent 90 trials per session in the two-odors task and 100 trials in the four-odors task, which kept the total session time < 40 minutes, an empirical value in which mice showed consistent engagement in the task. To enhance engagement of the animal in the task, we started each session in the discrimination phase by three consecutive presentation of the rewarded odor(s), where we kept the trial structure, however we presented a reward after the cue-window unconditionally of the animal’s licking behavior.

During optogenetic silencing we inhibited dCA2 PNs by activating inhibitory archaerhodopsin expressing in dCA2 of Amigo2-Cre mice by shining light (10 mW laser output, 532 nm) one seconds before odor onset, lasting two seconds into the inter-trial-interval to inhibit both, encoding and recall processes.

Two-photon calcium imaging

Imaging was performed using a galvo-galvo (Cambridge Technologies) based, two-channels Scientifica scope. Acquisition was performed with a long working distance Olympus 20x air lens (LCPL20XIR, 0.45 NA, 8.93 - 8.18 mm WD). A Mai Tai laser (Spectra Physics) tuned to 920 nm delivered 50-100 mW of excitation power at the front end of the lens. Emitted fluorescence was detected using a GaAsP detector on the green channel and a bialkali on the red one (MDU-PMT-50-00 Small B.A GaAsP and 2PIMS-PMT-40, respectively; Scientifica/Hamamatsu). Scanimage 5 was used for hardware control and data acquisition.

For each animal we acquired a z-stack spanning 50 μ m, centered at the imaging plane before the first recording session. This allowed us to take advantage of Scanimage’s correlation based online ‘motion-estimator’ module to find the exact field-of-view on each recording day with micrometer precision. In addition, it allowed to check x-, y-, and z-drift online, which we occasionally corrected manually during a recording session if it exceeded the threshold of 5 μ m. A field-of-view covered ~200 by 200 μ m and we scanned at 14 Hz. Both green and red signals were recorded, with the latter serving as input signal for software based offline image-alignment and motion correction.

Odor exploration in freely moving animals

For three days, each of five naïve female mice was habituated to an open square polyethylene field (24" L x 24" W x 12" H) for five minutes. The field contained two wire cups with filter paper (VWR, 9 cm diameter) clamped between the wires on opposite corners of the arena. After the third habituation, mice were subjected to a three-trial preference test. In each trial, 10 μ L of mouse urine (1:10 dilution in water; Urine G and E dilutions were prepared fresh from a frozen aliquot on the day of the experiment; Urine H was prepared three days prior to the experiment and kept at 4°C in the dark to test for potential degradation of the ‘attractiveness’ of the urine sample) was deposited on one filter paper in one corner and 10 μ L of a monomolecular odor dilution was deposited on the other filter paper. The dilution of the monomolecular odors was as follows: methyl butyrate, 1:2000; ethyl acetate, 1:250; and propyl propionate, 1:10 in mineral oil. Odor samples were placed randomly across trials to avoid spatial bias. Each trial lasted five minutes and mice trajectories were recorded for offline analysis. The inter-trial period for each mouse was one hour.

QUANTIFICATION AND STATISTICAL ANALYSIS

Signal extraction

Offline image registration and non-rigid motion correction, identification of regions of interest (ROIs), segmentation, and extraction of fluorescence signal were performed using the Suite2p software.⁵³ This package implements single day image registration and fluorescence source and neuropil detection from spatially overlapping ROIs. All identified ROIs were confirmed by manual inspection. Suite2p also provides a principal component analysis-based motion estimator module,⁵⁷ which allows to qualitatively detect even subtle remaining drifts after offline motion correction. We only included animals with stable window implants where we could not detect motion drifts after correction. ROIs were excluded where we detected nuclear expression of GCaMP, a sign of toxicity caused by overexpression.

Longitudinal registration

For day-to-day longitudinal cell registration, we used a pipeline reported earlier.²⁹ Briefly, the approach uses a three-step procedure: first, it performs rigid alignment between the field of views of different imaging sessions based on the identified ROIs; second, it models the distribution of spatial proximities between pairs of neighboring cells from different sessions to obtain an estimation for their probability to be the same cell (either based on the centroid distance or alternatively the spatial correlation of ROIs); third, it registers cells across multiple sessions using clustering to obtain probabilities of neighboring cell-pairs to be the same cell. Spatial correlation, using a threshold of 0.5, worked best with our data.

Data processing

Extracted fluorescent traces were neuropil subtracted (scaling factor for neuropil: 0.7) and slow baseline trends were corrected by subtracting the 8th percentile within a 30 second window as reported earlier.²⁴ Each cell's detrended activity traces were individually scored by their median absolute deviation (MAD) using MATLAB's *normalize* function. To visualize high-dimensional data using principal component analysis, we achieved better results by additionally correcting for baseline differences in expression level using a framework described earlier.⁵⁸ Briefly, we additionally re-normalized signals by dividing each neuron's signal by the sum of its maximum value during a session and the 95th percentile of the signal across all neurons. This way, we reduced major differences between strongly and weaker expressing cells but kept priority for larger transients. To align signals from the microscope with behavioral data, which were sampled at different frequencies (14 Hz and 20 Hz respectively), we aligned signals using nearest-neighbor-interpolation and re-sampled at 10 Hz.

Respiration sampling

Respiration traces were filtered using a second order Savitzky-Golay filter in 100 ms-long windows.

Data analysis

Data analysis was performed using custom-written code in MATLAB.

ROC analysis

To detect significant modulation of a cell above baseline fluctuations, we used receiver-operator-characteristic (ROC) analysis. We generated two activity distributions, the average fluorescent activity for each trial of a respective cell-odor pair in a 3-second time window before ($t = 1\text{--}4\text{ s}$ during a given trial) and after ($t = 6\text{--}9\text{ s}$) odor presentation. The resulting two activity distributions were subjected to ROC analysis, and we computed the area-under-the-receiver-operator-curve statistic (AUC) (see also Figure S1) to derive the selectivity-index (SI) as: $2 * (\text{AUC} - 0.5)$. The index is bound between -1 and 1. A value of 0 indicates no bias to either baseline or post-odor presentation. A value below 0 shows higher activity during baseline, whereas values larger than 0 show a higher activity after odor presentation. To determine the significance, we sampled under the null-hypothesis (no difference between the distributions) and re-calculated a selectivity index. We repeated this 1000 times, which provided for each cell-odor pair a selectivity-index distribution. A significant response was defined whenever the experimental SI was either below the 2.5th percentile, which we considered an odor-inhibited cell, or above the 97.5th percentile, which we considered an odor-activated cell, of the shuffled distribution.

PCA analysis

For principal component analysis (PCA) we focused only on the average activity during the 3 s after odor presentation (post-odor period). We constructed a data matrix with individual cells in columns and concatenated the averaged normalized response in the post-odor period for each trial along rows (e.g., with two odors and control trials, 30 repetitions each, and one averaged activity data point per trial this resulted in 90 data points/rows for each cell). We then calculated the cell-by-cell covariance matrix and used PCA analysis to identify the eigenvectors of the covariance matrix. Using the resulting eigenvectors, we obtained the principal components by projecting our original data into the principal component (PC) space.

To fit a PCA model to data comprising multiple session, we restricted our analysis to cells that were reliably identified across days. We averaged individual trial activity as described above, however, to fit the PCA model we concatenated all trials across multiple days into a large multi-day trial-by-cell activity matrix. We then performed PCA to receive the eigenvectors and projected trial activity from individual sessions into the multi-day PC space.

We plotted either the first two or three PCs, where each data point indicates the averaged post-odor activity for a given trial. Color coding was done post hoc based on the trial identity. For visualization purposes we added a Gaussian fit to each stimulus cluster.

Decoder analysis

For binary decoders, we implemented a Support Vector Machine (SVM) performing C-Support Vector Classification with a linear kernel using the LIBSVM MATLAB implementation.⁵⁹ We used five-fold cross-validation throughout our decoding analysis. The regularization hyperparameter C was selected using a random search on a separate validation set and we chose a less permissive value of 50 for all experiments. To decode across a single-trial time-course, we averaged fluorescent data within half overlapping bins using a bin size of 200 ms and trained and tested a separate decoder on each bin. Chance decoding for stimulus decoding (not for CCGP, see below) was accomplished by randomly shuffling trial identity ($n = 1000$). Results were calculated as average accuracy across

folds and across animals in cases where we focused on individual animals rather than a pseudo population. When decoding based on pseudo population activity, significance above chance was determined by first averaging across the post-odor period (6–9 seconds) to obtain the average post-odor decoding accuracy. Chance decoding under the null hypothesis (randomly shuffled trial identity), yielded a mean null decoding performance (μ_{Null}) and standard deviation of the null distribution (σ_{Null}). The p value was then derived from the z-score of the average post-odor decoding accuracy (μ_{Data}) compared with the chance distribution: $Z = (\mu_{\text{Data}} - \mu_{\text{Null}}) / \sigma_{\text{Null}}$.

To test for statistical significance across individual animals, we first obtained average signal and chance decoding accuracies in the 3-s post odor window for each animal individually. We then pairwise subtracted signal and chance and took the mean of the resulting accuracy differences to obtain a single expected mean decoding difference between signal and chance. We compared this expected mean difference value against a bootstrapped ($n = 10000$) distribution of mean differences under the null hypothesis of zero-mean difference.⁶⁰ Briefly, given that x and y are vectors containing the average signal and chance decoding accuracies for individual animals respectively, we created two new data sets $x'_i = x_i - \bar{x} + \bar{z}$ and $y'_i = y_i - \bar{y} + \bar{z}$ where \bar{z} is the mean of the combined sample. The distribution of mean differences under the null hypothesis was then obtained by bootstrapping from the pairwise difference distribution $x' - y'$. The corrected empirical p-value⁶¹ was then calculated as: $(r + 1)/(n + 1)$, with r being the number of values from the null distribution that are smaller/larger (depending on the hypothesis) than the expected mean difference accuracy and n the total number of bootstrap samples.

For the generalized decoder, which determines the cross-categorization performance (CCGP),³¹ we trained and tested in two opposite directions: we first trained decoder-models across time to classify odor pair one (e.g., reward vs. non-reward or social vs. non-social) and tested the trained models on the remaining odor (odor pair two) (see also Figures S7 and S9 for a schematic illustration). This way, the trained model is naïve with respect to the testing data. In the second direction we trained and tested in the opposite direction (train: pair two, test: pair one). This bidirectional training/testing accounts for asymmetry in the data.

To estimate a meaningful null model for CCGP we aimed to preserve individual stimulus decoding while selectively randomizing structure in the activity data that underlies generalization.³¹ To achieve this, we performed a trial-class-based rotation-translation of the activity vectors by randomly shuffling the neuron index within each trial class. We computed the CCGP as described above to obtain a null model of the CCGP value and repeated this 1000 times. The significance of the CCGP values from the experimental data in individual animals was computed with respect to their averages of the null model CCGPs based on mean-difference using bootstrap-based testing as described above.

When we had more than two classes to predict, we used a decoding approach based on the Euclidean distance of the population vectors. We first binned the data using 200 ms bins. For each bin, using five-fold cross validation, we trained a model by calculating the average population vector for the responses to each odor and the blank air in n -dimensional neuron-activity space (n = number of neurons, e.g., training in the two odors plus one blank paradigm resulted in three average population vectors) in the training set. We then calculated for each trial in the test set its Euclidean distance to the respective average population vectors. The class with the smallest distance became the predicted odor for this trial. We calculated the empirical p-value as described above.

Fisher's Exact Test

To test for significant differences in the frequency of cells being modulated by odor compared with control trials we performed for individual odors a Fisher's Exact Test on the two-by-two contingency table using a MATLAB implementation (Cardillo G., 2007; MyFisher22: a very compact routine for Fisher's exact test on 2x2 matrix).

The same function was used to test for a significant association between the learning of a reward association and the frequency of cells being tuned to the rewarded and the non-rewarded odor respectively.

Logistic model

To characterize the behavioral learning curve for odor association with a water reward, we used MATLAB's *fit* (the following parameters were used: Method, *NonlinearLeastSquare*; Algorithm, *Trust-Region*; MaxIter, 1e6; UpperConstraint, [1 Inf Inf]; LowerConstraint, [0 0 0]) and *coeffvalues* functions to fit a three-parameters logistic model to the data: $a/(1 + \exp(-b * (x - c)))$, with a being the plateau value, b the slope, and c the midpoint point of the model. In cases where we tested for significance, we used Monte-Carlo random sampling testing. We randomly assigned values from the treatment and control group, fitted the model, and saved the resulting coefficients. We repeated this 5000 times, which resulted in a distribution of coefficients, and then calculated the one-sided, corrected empirical p-value by: $(r + 1)/(n + 1)$, with r being the number of values from the shuffled distribution that are either smaller or larger (depending on the hypothesis) than the observed value and n the total number of repetitions, in this case 5000.

Trajectory analysis and analysis of odor exploration time

Mice trajectories during freely moving exploration were extracted through pose estimation with DeepLabCut.⁵⁴ Trajectories served for visualization purposes only. The exploration time of odors was quantified by researchers who were blind with respect to the odor identity during analysis and independent from the researcher who conducted the task. Only active exploration (mouse's head towards the cup with the filter) was counted. Scoring was done using Behavioral Observation Research Interactive Software.⁵⁵